

Free-electron Optical Nonlinearities in Plasmonic Nanostructures: A Review of the Hydrodynamic Description

Alexey V. Krasavin,* Pavel Ginzburg, and Anatoly V. Zayats

Requirements of integrated photonics and miniaturisation of optical devices demand efficient nonlinear components not constrained by conventional macroscopic nonlinear crystals. Intrinsic nonlinear response of free carriers in plasmonic materials provides opportunities to design both second- and third-order nonlinear optical properties of plasmonic nanostructures and control light with light using Kerr-type nonlinearities as well as achieve harmonic generation. This review summarises principles of free-carrier nonlinearities in the hydrodynamic description in both perturbative and non-perturbative regimes, considering also contribution of nonlocal effects. Engineering of harmonic generation, solitons, nonlinear refraction and ultrafast all-optical switching in plasmonic nanostructures and metamaterials are discussed. The full hydrodynamic consideration of nonlinear dynamics of free carriers reveals key contributions to the nonlinear effects defined by the interplay between a topology of the nanostructure and nonlinear response of the fermionic gas at the nanoscale, allowing design of high effective nonlinearities in a desired spectral range. Flexibility and unique features of free-electron nonlinearities are important for nonlinear plasmonic applications in free-space as well as integrated and quantum nanophotonic technologies.

1. Introduction

Nonlinear regime of interaction of light and matter became accessible with the development of lasers. Despite nonlinear effects being weak and requiring high intensities of light to be observed, nonlinear optics enables numerous important applications in modern technologies from harmonic generation, optical parametric amplification and mode-locking in ultrafast lasers to holography, self- and cross-modulation of optical signals, and optical solitons for information processing, as well as parametric down-conversion for quantum information applications. Due to the weakness of the nonlinear response of conventional

materials, only selected, *nonlinear* materials exhibit considerable nonlinear optical effects at reasonable light intensities, and typically a long propagation length in a material is needed to achieve significant nonlinear effects.^[1,2]

Recent development of integrated optics and miniaturisation of optical components and devices put forward new challenges for nonlinear optics at the (sub)wavelength scales, where geometrical constraints limit the applicability of conventional macroscopic nonlinear crystals and approaches which rely on phase matching or long interaction length between optical beams. At the same time, nonlinear effects are essential for optical signal processing in photonic integrated circuits.

In order to increase the efficiency of light-matter interactions in a linear domain, plasmonic modes in conductors and their nanostructures, including metal-dielectric metamaterials, have

recently been widely used.^[3–9] Plasmonic excitations, either propagating surface plasmon polaritons (SPPs) on extended metal surfaces or localised surface plasmons (LSPs) in metallic nanoparticles, are related to a coupled state of photons and coherent free-carrier oscillations near a conductor-dielectric interface. Plasmonic excitations provide electromagnetic field confinement near the interface and, as the result, the local field enhancement. This has profound consequences for nonlinear optical processes which depend on the local field intensity in a superlinear manner and, thus, can be strongly enhanced near the metal-dielectric interface in the presence of plasmonic resonances.^[10,11]

Nonlinear plasmonics has been developed utilising the above-described properties of plasmonic field, while also taking advantage of the nanoscale range of plasmonic modes enabling to achieve nonlinear response on subwavelength scales and, thus, being naturally compatible with integrated optics. There are two typical approaches: (i) to use the field enhancement provided by surface plasmons to induce a nonlinear response in nonlinear dielectric near the metal interface in hybrid metal-dielectric systems or (ii) to harvest the nonlinearity of plasmonic materials themselves. In the latter case, a nonlinear response originates from the dynamics of non-equilibrium free-electrons in the medium under the influence of strong electromagnetic field of the illumination. Indeed, the metal nonlinear response is one of the strongest per unit interaction length and fastest, with the

Dr. A. V. Krasavin, Prof. A. V. Zayats
Department of Physics
King's College London
Strand, London WC2R 2LS, United Kingdom
E-mail: alexey.krasavin@kcl.ac.uk

Dr. P. Ginzburg
School of Electrical Engineering
Tel Aviv University
Ramat Aviv, Tel Aviv 69978, Israel

 The ORCID identification number(s) for the author(s) of this article can be found under <https://doi.org/10.1002/lpor.201700082>

DOI: 10.1002/lpor.201700082



Alexey V. Krasavin received his B.Sc. (with honors) and M. Sc. (with honors) degrees from Moscow Institute of Physics and Technology. In 2006, he received PhD in Physics from the University of Southampton and joined Queen's University Belfast as a post-doctoral research fellow. Since 2010 he works in King's College London. His research interests include active ma-

nipulation and amplification of plasmonic signals in highly-integrated optical circuits, nonlinear plasmonic-assisted effects, plasmonic-enhanced fluorescence and optical metamaterials.



Pavel Ginzburg is a Senior Lecturer at Tel Aviv University. He is a former EPSRC Research Fellow, International Newton Research Fellow, and Rothschild Fellow at King's College London. He obtained his degrees in Electrical Engineering at Technion. His PhD thesis was awarded with a QEOD Thesis Price for Applied Aspects. Nowadays, Pavel holds a prestigious Alon Fellow-

ship and is the head of 'Dynamics of Nanostructures' Laboratory, encompassing a theoretical group, optical spectroscopy and radio waves labs. Pavel has authored 56 journal papers, over 100 conference presentations and 2 patents.



Anatoly V. Zayats is the head of Photonics & Nanotechnology Group at the Department of Physics, King's College London. He graduated and received PhD in Physics from Moscow Institute of Physics and Technology. His current research interests are in the areas of nanophotonics and plasmonics, metamaterials, nonlinear optics and spectroscopy. He is a holder of the

Royal Society Wolfson Research Merit Award, a Fellow of the Institute of Physics, the Optical Society of America, SPIE and The Royal Society of Chemistry.

femtosecond-scale response time determined by relaxation of the excited electrons to the equilibrium state, governed primarily by electron-electron and electron-phonon scattering. Both approaches were exploited for enhancement of coherent nonlinear interactions, such as harmonics generation and wave mixing, as well as Kerr-type nonlinearities for controlling light with light. The latter is a third-order nonlinear effect leading to the modification of permittivity of the material and is manifested in self- or cross-phase modulation and induced transparency or absorption.

Here, we will overview principles of free-electron nonlinearities in plasmonic nanostructures and their applications. A full hydrodynamic model of free-electron nonlinearities will be de-

scribed to address coherent as well as Kerr-type nonlinearities of metals. We discuss, in turn, engineering of harmonic generation, nonlinear refraction and ultrafast all-optical switching in metallic nanostructures and plasmonic metamaterials, taking into account nonlocal response as well as the behaviour in the so-called epsilon-near-zero regime. Finally, nonlinear surface plasmon polaritons and plasmon-solitons will be briefly introduced.

2. Free-electron Dynamics in Plasmonic Nanostructures

2.1. Linear Free-electron Dynamics

Optical properties of materials with high concentration of free carriers (electrons or holes), such as metals or highly doped semiconductors, as well as their films and nanostructures are governed by coupling of electromagnetic field to the coherent motion of free-carrier plasma. Comprehensive description of the carrier dynamics in a quasi-classical approach can be established considering a set of hydrodynamic-type equations treating the electron plasma as a charge fluid.^[12–15]

$$m(\partial_t \mathbf{v} + \mathbf{v} \cdot \nabla \mathbf{v}) + \gamma m \mathbf{v} = -e(\mathbf{E} + \mathbf{v} \times \mathbf{H}) - \nabla p/n, \quad (1)$$

$$\partial_t n + \nabla \cdot (n\mathbf{v}) = 0, \quad (2)$$

where n and \mathbf{v} are the hydrodynamic variables representing the carrier density and velocity, respectively, e and m are the electron charge and mass, respectively, γ is the electron scattering rate, \mathbf{E} and \mathbf{H} are the local electric and magnetic fields, respectively. In particular, the hydrodynamic model includes terms describing convective acceleration $\mathbf{v} \cdot \nabla \mathbf{v}$, Lorentz force $e n \mathbf{v} \times \mathbf{H}$ and quantum pressure $\nabla p/n$, the latter giving rise to nonlocal effects in both linear and nonlinear responses. The hydrodynamic electron dynamics can be derived from the Boltzmann equation^[13,16] or from density functional formalism^[12,17], its advanced description can be obtained from quantum mechanical calculations.^[18] The quantum pressure $\nabla p/n$, can be evaluated within the Thomas-Fermi theory of an ideal fermionic gas with p given by [12,14]

$$p = (3\pi^3)^{2/3} \frac{\hbar^2}{5m} n^{5/3}. \quad (3)$$

When treating the linear behaviour of the electron gas, the non-local term $\nabla p/n$ in Eq. (1) is frequently represented after linearisation as $m\beta^2 \nabla n/n_0$, where β is the spatial dispersion parameter and n_0 is the equilibrium electron density. How to determine a value of β^2 was a topic of extended discussions (for a comprehensive overview see Ref. [12]). For low frequencies ($\omega \ll \gamma$), from the Thomas-Fermi theory, $\beta^2 = \frac{(3\pi^3)^{2/3}}{3} \frac{\hbar^2}{m^2} n_0^{2/3} = \frac{v_F^2}{3}$, where v_F is the Fermi velocity. At high frequencies ($\omega \gg \gamma$), $\beta^2 = \frac{3v_F^2}{5}$ represents the dynamic pressure.^[12]

The hydrodynamic treatment was first used by Ritchie in his seminal work,^[19] where he predicted the existence of surface plasmons. Considering the behaviour of the free-carrier gas in a plasmonic nanostructure under illumination with an electro-

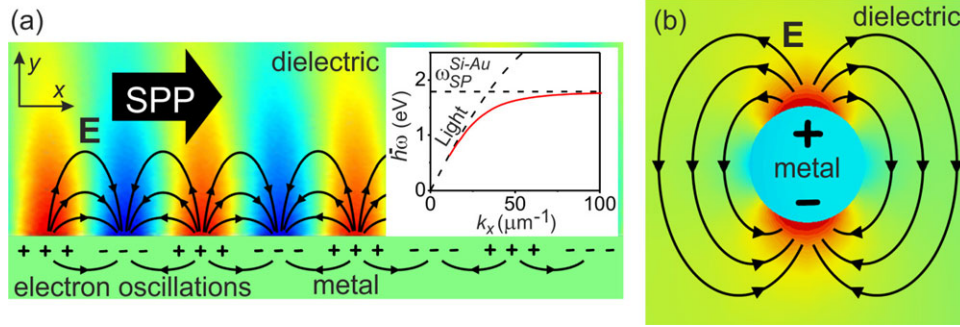


Figure 1. a) Snapshot of the electric field (E_y colour map and E field lines) of a surface plasmon polariton wave propagating along the interface between a metal and a dielectric, together with the related charge distribution. Inset shows the SPP dispersion at a Si/Au interface. b) Snapshot of the electric field of a localised surface plasmon produced by oscillating charges in a metal nanoparticle.

magnetic wave, the optical response can be calculated with a help of Eqs. (1) and (2). For a finite height of the potential well in which the gas is located, the quantum effects related to spill-out of an electron gas in the potential barrier become important.^[20,21] The hydrodynamic model combined with the additional Lorentzian resonance terms, which describe the contributions from the interband transitions present in a medium, is capable to reproduce metal susceptibilities over the entire spectral range.^[22] The mesoscopic hydrodynamic approach is integrable with electromagnetic modelling, enabling studies of large-scale electromagnetic systems with nontrivial geometries. It is worth noting that *ab initio* microscopic models while providing more quantitative results^[23,24] are extremely time-consuming due to the computation complexity involved^[25] and in many cases limited to a low number of considered atoms, addressing the systems much smaller than accessible experimentally in vast majority of cases. Therefore, it is not surprising that the hydrodynamic model, much more robust from this point of view, was often and successfully applied to reveal a vast variety of nanoscale optical phenomena involving materials with free carriers.

In the first approximation, the terms responsible for convection, Lorenz and nonlocal response are usually dropped out, and the dynamics of free-electron gas under the excitation by an electromagnetic wave at a given frequency ω is described by the equation:

$$m n \partial_t \mathbf{v} + \gamma m n \mathbf{v} = -e n \mathbf{E}, \quad (4)$$

where $\mathbf{E} = \mathbf{E}_0 \exp(i\omega t)$ is the electric field component of the wave. This is a linear differential equation and, thus, the response of the electron gas is linear and harmonic, described by the displacement $\mathbf{r} = \mathbf{r}_0 \exp(i\omega t)$, with $\partial_t \mathbf{r} = \mathbf{v}$. Knowing the displacement, it is easy to obtain the resulting equivalent dielectric polarisation of the gas, and finally the permittivity of the metal, which is given by the well-known Drude formula

$$\varepsilon_D^{free}(\omega) = 1 - \frac{\omega_p^2}{\omega^2 + \gamma\omega i}, \quad (5)$$

where $\omega_p = \sqrt{ne^2/(m\varepsilon_0)}$ is the plasma frequency. Introducing the permittivity related to core electrons $\varepsilon_{core}(\omega)$ which takes into

account the interband transitions, it can be rewritten as

$$\varepsilon_D(\omega) = \varepsilon_{core}(\omega) - \frac{\omega_p^2}{\omega^2 + \gamma\omega i}. \quad (6)$$

A direct consequence, easily seen from Eq. (6), is the peculiarity of optical properties of metal, when below a certain frequency the second term becomes greater than the first one, making the overall dielectric permittivity negative. This, in turn leads to the appearance of electromagnetic excitations specific to metallic nanostructures: localised surface plasmons and surface plasmon polaritons.

Surface plasmon polariton is a propagating surface wave at the continuous metal-dielectric interfaces (Figure 1a). The SPP electromagnetic field has components both perpendicular to the metal surface and parallel to it (along the wavevector $k(\omega)$) and exponentially decays on both sides of the interface, providing sub-wavelength confinement.^[4,26] The SPP dispersion is given by

$$k(\omega) = \frac{\omega}{c} \sqrt{\frac{\varepsilon_d \varepsilon_D(\omega)}{\varepsilon_d + \varepsilon_D(\omega)}}, \quad (7)$$

where ε_d is the permittivity of the dielectric adjacent to the metal.^[4,26] The dispersion of SPP waves calculated using the Drude formula (Eq. (5)) for the metal permittivity is presented in the inset to Figure 1a. At low frequencies, it is very close to the dispersion of light in the adjacent dielectric, corresponding to a weakly bounded surface wave, then passing through the truly polaritonic regime at high k asymptotically approaches $\omega_{SP} = \omega_p / \sqrt{1 + \varepsilon_d}$ line corresponding to non-propagating surface plasmons. As can be easily seen, SPP has a wave vector larger than that of a photon, which means that SPP is a slow wave accumulating energy from incoming photons and providing the field enhancement near the metal interface compared to the field of the incident light. The SPP dispersion and, therefore, the field confinement and enhancement can be modified by structuring the interface, either metal or dielectric medium, thus achieving plasmonic waveguides (structuring across the SPP propagation direction)^[5,27] or plasmonic crystals (structuring in the plane of the SPP propagation).^[4]

Localised surface plasmons (LSPs) are associated with the electron plasma oscillations in confined (subwavelength) geometries, e.g., metal nanoparticles (Figure 1b). LSP resonances

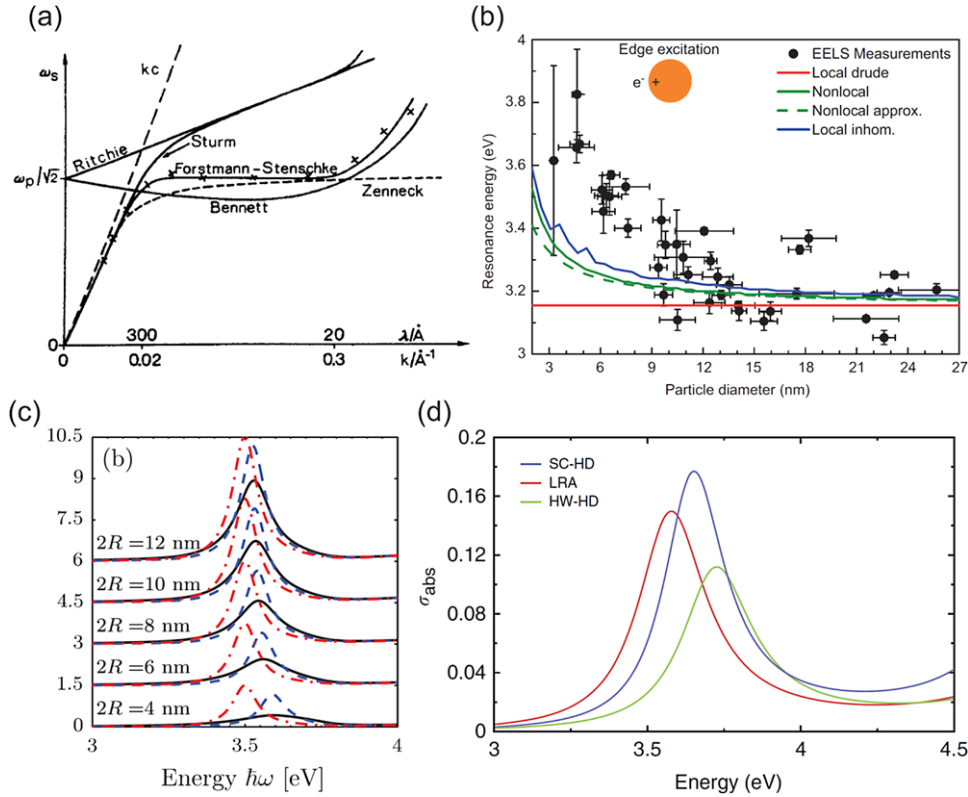


Figure 2. a) SPP dispersion in various approximations. Crosses correspond to the experimental data for Al. Reproduced with permission.^[13] Copyright 1986, Springer-Verlag. b) Position of a surface plasmon resonance as a function of the nanoparticle diameter. Reproduced with permission.^[35] Copyright 2013, Science Wise Publishing and De Gruyter. c) Extinction cross-section (normalised to the geometrical cross-section πr^2) of an Ag nanoparticle of decreasing radii calculated using: local response approximation (red dash-dotted lines), hydrodynamic model (blue dashed lines) and GNOR hydrodynamic model (black solid lines). Reproduced with permission.^[33] Copyright 2015, IOP Publishing. d) Absorption cross-section spectra for an Ag nanoparticle with $r = 1.5$ nm calculated using: LRA – local response approximation, HW-HD – hard wall hydrodynamic model, SC-HD – self-consistent hydrodynamic model which takes into account the spill-out effect. Reproduced with permission.^[39] Copyright 2015, Macmillan Publishers Limited.

depend on the particle size, shape and refractive index of surroundings. LSPs can be resonantly excited with light of the appropriate frequency irrespectively of the excitation light wavevector. For example, the fundamental dipolar plasmonic resonance of a spherical particle with a size much smaller when the wavelength corresponds to a dramatic increase in its polarisability:

$$\alpha(\omega) = 4\pi R^3 \frac{\epsilon_D(\omega) - \epsilon_d}{\epsilon_D(\omega) + 2\epsilon_d}, \quad (8)$$

which is defined by a minimum of the denominator and happens at the frequency approximately given by

$$\text{Re}[\epsilon_D(\omega_{LSP})] = -2\epsilon_d. \quad (9)$$

Since LSPs are confined near the nanoparticle, they have a small mode volume and, therefore, provide a significant electromagnetic field enhancement, which is limited in the first approximation by their quality factor determined by Ohmic and radiative losses, as well as nonlocal effects in the case of ultrasmall sizes.

The advanced description provided by the full hydrodynamic Eqs. (1)–(3) is more complicated. If all the equations are linearised, then for a plane wave propagating along an *arbitrarily-*

chosen z direction, the hydrodynamic permittivity presents a tensor^[12]

$$\epsilon_m = \text{diag}(\epsilon_T, \epsilon_T, \epsilon_L). \quad (10)$$

Here, the tensor signifies different permittivity values for the transverse and longitudinal electric field components allowed in the medium, while the medium is strictly isotropic, $\epsilon_T = \epsilon_\infty - \frac{\omega_p^2}{\omega^2 + \gamma\omega i}$ and $\epsilon_L = \epsilon_\infty - \frac{\omega_p^2}{\omega^2 + \gamma\omega i - \beta^2 k^2}$ with $\epsilon_\infty = \epsilon_{core}(\omega \rightarrow \infty)$ being the high-frequency permittivity of the metal and for the simplicity the frequency dependence of $\epsilon_{core}(\omega)$ was omitted. Applying this model to the surface plasmons and taking for simplicity $\gamma = 0$ (lossless case) and $\epsilon_\infty = 1$, it can be found that the nonlocal corrections bring essential modifications to the high-frequency (surface plasmon) part of the SPP dispersion, which becomes dependent on the wave vector:^[12,28–31]

$$\omega = \frac{\omega_p}{\sqrt{2}} \left(1 + \frac{\beta k}{\sqrt{2}\omega_p} \right), \quad (11)$$

which is the Ritchie formula. Typical metals and semiconductors exhibit self-consistent changes of the electron densities near the surface, which leads to a more sophisticated plasmonic

dispersion models showing a good agreement with the experimental data (Figure 2).^[12,32]

In the past, optical properties of mainly bulk and macroscopic objects were studied and the Drude description was proven to faithfully describe their properties. With the availability of metal nanostructures and nanoparticles, with their subwavelength characteristic sizes, the deviations from the Drude model become more pronounced due to the increased relative contribution of other terms in the hydrodynamic model (Eq. (1)), which is especially pronounced when considering nonlinear response of the nanostructures. However, the full hydrodynamic description given by Eqs. (1) and (2) also proved to be an invaluable tool for understanding linear optical properties of metallic nanostructures, particularly when their size reaches truly nanometric scale.^[33,34] In this case, the Lorenz and convection terms in Equation (1) are omitted, as purely nonlinear, while the quantum pressure term is linearised to the form $m\beta^2\nabla n/n_0$ and being proportional to the gradient of the carrier density introduces nonlocal corrections. The influence of nonlocality, particularly dramatic in nanoscale geometries, can already be seen in the most classical example of plasmonic resonances in metallic nanoparticles, resulting in their essential blue-shift as the radius of the nanoparticle r approaches 5 nm (Figure 2a).^[35–37] In the full hydrodynamic description this can be successfully described by the resulting modification of the nanoparticle polarisability^[35]

$$\alpha^{NL}(\omega) = 4\pi r^3 \frac{\varepsilon_D(\omega) - \varepsilon_d \cdot (1 + \delta_{NL})}{\varepsilon_D(\omega) + 2\varepsilon_d(1 + \delta_{NL})}, \quad (12)$$

by a nonlocal correction

$$\delta^{NL} = \frac{\varepsilon_D(\omega) - \varepsilon_{core}(\omega)}{\varepsilon_{core}(\omega)} \frac{j_1(k_L r)}{k_L R j_1'(k_L r)}, \quad (13)$$

where

$$k_L = \sqrt{\omega^2 + \omega\gamma i - \omega_p^2/\varepsilon_{core}(\omega)/\beta} \quad (14)$$

is the wavenumber of an additional wave, now allowed to be excited in the nanoparticle, and j_1 is the spherical Bessel function of the first order. The excitation frequency of the dipolar resonance is given by the pole of polarisability in Eq. (12):

$$\text{Re}(\omega_{LSP}^{NL}) = \frac{\omega_p}{\sqrt{3}} + \frac{\sqrt{2}\beta}{2r}, \quad (15)$$

where air was taken as the surrounding medium. Thus, the influence of the nonlocality increases with the size decrease. Figure 2b shows that the resonant shift derived from the hydrodynamic theory describes the experimental results obtained by electron energy-loss spectroscopy very well.

In the generalized nonlocal optical response (GNOR) hydrodynamic model^[33,38], an electron diffusion term $eD\nabla n$ (D is the diffusion constant) is incorporated in the continuity Eq. (2), resulting in a well-known convection-diffusion equation

$$\partial_t n + \nabla \cdot (nv) - D\nabla^2 n = 0. \quad (16)$$

The constitutive relation between the current $\mathbf{J} = -en\mathbf{v} + eD\nabla n$ and the electric field \mathbf{E} can be determined after linearisation of Eqs. (1) and (16):

$$\left[\frac{\beta^2}{\omega(\omega + i\gamma)} + \frac{D}{i\omega} \right] \nabla(\nabla \cdot \mathbf{J}) + \mathbf{J} = \sigma_D \mathbf{E}, \quad (17)$$

where $\sigma_D = i\varepsilon_0\omega_p^2/(\omega + i\gamma)$ is the usual Drude conductivity. If GNOR is applied to a plasmonic resonance in a metallic nanoparticle, the first term in the nonlocal term pre-factor leads to a shift in the resonance position (returning Eq. (15)), while the second, diffusion-related term, leads to a correction to the imaginary part of the dipolar resonant frequency

$$\text{Im}(\omega_{LSP}^{NL}) = -\frac{\gamma}{2} + \frac{\sqrt{6}}{12} \frac{D\omega_p}{\beta r}, \quad (18)$$

resulting in the increase of a resonant peak width (Figure 2c)^[33] (as confirmed with the authors of References^[33] and^[38], the correct coefficient in the second denominator of Eq. (18) is 12 and not 24 as in Ref. 38). It must be stressed that the correction related to the broadening has a purely nonlocal nature and is not related to any modification of the dissipative term $\gamma m\mathbf{v}$, which is incorporated in σ_D . Within the same approach, the requirement of an infinitely high potential barrier at the nanostructure boundaries (a hard-wall condition) can be relaxed, allowing for the electron spill-out effects, which leads to further elaboration of the LSP resonance position. In this respect, it was shown that the nonlocal correction and the spill-out effects have counteracting influences (Figure 2d).^[39,40] In the treatment of the spill-out effects careful consideration should be given to the calculation of the spatial dependence of the equilibrium electron density, to which the results are very sensitive.^[41]

Other examples of linear nonlocal hydrodynamic effects include the modification of the molecular fluorescence^[42] as well as the plasmonic field confinement and enhancement^[43–46], the latter effects lead to the re-evaluation of SERS efficiency^[47] and are also important in the context of nonlinear optics. For a recent review on the linear nonlocal hydrodynamic phenomena we refer the reader to Ref. [33].

2.2. Nonlinear Free-Electron Dynamics

It is in nonlinear optics where the hydrodynamic description plays the crucial role, since the electron gas acts as the very source of the nonlinearity. Indeed, the interaction of electromagnetic fields with nano-objects made of arbitrary nonmagnetic materials is described in terms of the induced polarisation $\mathbf{P}(\mathbf{r}, t)$ via the wave equation^[48]

$$\nabla \times \nabla \times \mathbf{E}(\mathbf{r}, t) + \frac{1}{c^2} \partial_{tt} \mathbf{E}(\mathbf{r}, t) + \mu_0 \partial_{tt} \mathbf{P}(\mathbf{r}, t) = 0, \quad (19)$$

where $\mathbf{E}(\mathbf{r}, t)$ is the electric field, c is the speed of light in vacuum, and μ_0 is the vacuum permeability. In general, the spatio-temporal polarisability holds all the information on both linear and nonlinear responses of the material, also including its

chromatic dispersion. The polarisability of plasmonic structures can be introduced in Eq. (19), via natural hydrodynamic variables: the macroscopic position-dependent electron density $n(\mathbf{r}, t)$ and velocity $\mathbf{v}(\mathbf{r}, t)$, which are subsequently related to the polarisation current as

$$\partial_t \mathbf{P} = \mathbf{J} = -en\mathbf{v}. \quad (20)$$

The crucial observation is that the full hydrodynamic description for the polarisation leads to inherently nonlinear behaviour. As it follows from Eqs. (1) and (2), which are nonlinear in their nature in terms of the hydrodynamic variables n and \mathbf{v} , the harmonic excitation of a free-electron gas results in the generation of higher harmonics in the polarisation current \mathbf{J} described by n and \mathbf{v} . The harmonics are further intermixed in the resulting electronic polarisation (Eq. (20)), which acts as a source term for the generation of nonlinear harmonic fields (Equation (19)). The set of nonlinear hydrodynamic equations (Eqs. (1) and (2)) provides a self-consistent formulation of nonlinear optical processes originating from free-carriers in plasmonic systems. The effects of both surface nonlinearities and nonlocality are taken into account via the boundary conditions imposed by the Maxwell's equations and vanishing current perpendicular to the metal boundaries. In a perturbative regime of light-matter interactions (weak pump field), the leading nonlinear polarisability is of the second order with respect to the hydrodynamic variables and is the result of the convective acceleration term $\mathbf{v} \cdot \nabla \mathbf{v}$, the magnetic component of the Lorentz force $-\mathbf{e}\mathbf{v} \times \mathbf{H}$, quantum pressure term $\nabla p/n$ in Eq. (1), and the $n\mathbf{v}$ term in Eq. (20)^[49] (see Section 4.1). Beyond the perturbative regime, at very high peak excitation powers, higher-order nonlinear terms in the hydrodynamic description of the electron gas need to be considered, resulting in the intermixing of bulk and surface nonlinear effects, which will be discussed in Section 6. The collective action of these terms ultimately defines the nonlinear optical response of metals and other plasmonic materials with high concentration of free carriers under visible and infrared light illumination, away from the spectral range of interband transitions. In particular, predictions of second-order nonlinear optical properties^[14,49] and Kerr-type nonlinearities,^[50] based on the hydrodynamic method, qualitatively agree with the experiments.

Universal properties of all types of plasmonic nanostructures important for nonlinear optical applications are (i) the field enhancement near the metal surface compared to the free space field of the exciting light, (ii) strong sensitivity to the refractive index changes near the metal surface,^[19] and (iii) possibility to engineer SPP mode dispersion or LSP resonances by controlling nanostructure geometry and dielectric surroundings. Thus, the resonant response can be tuned to the required operational wavelength where nonlinear response needs to be enhanced. Intrinsic nonlinearity of free-electron systems is also extremely fast with the response time determined by the electron relaxation within the conduction band,^[9] and, thus, provides opportunities for the implementation of ultrafast all-optical effects for modulating and switching of light with light.

3. Basic Notions of Nonlinear Optics

Nonlinear optical interactions are relatively weak and require high light intensities to observe. The field of the incident light can however be significantly enhanced by coupling it to material structures with a resonant electromagnetic response. In particular, the electromagnetic field of plasmonic excitations is localised at the sub-wavelength scales near metal-dielectric interfaces, that provides significant field enhancement and can boost nonlinear optical effects. Generally, nonlinear optical phenomena are proportional to higher powers of the driving field (e.g., a power of two for second harmonic generation (SHG) which is a second-order nonlinear process) and the induced polarisation can be expressed as^[2]

$$\mathbf{P}(\omega) = \mathbf{P}^{(1)}(\omega) + \mathbf{P}^{(2)}(\omega) + \mathbf{P}^{(3)}(\omega) + \dots \quad (21)$$

with

$$\mathbf{P}^{(1)}(\omega) = \varepsilon_0 \chi^{(1)}(\omega) \cdot \mathbf{E}(\omega), \quad (22)$$

$$\begin{aligned} \mathbf{P}^{(2)}(\omega) = \varepsilon_0 \chi^{(2)}(\omega = \omega_1 + \omega_2; \omega_1, \omega_2) : \mathbf{E}(\omega_1) \mathbf{E}(\omega_2) \\ + \mathbf{P}'^{(2)}(\nabla \chi^{(2)}, \nabla \mathbf{E}(\omega_1), \nabla \mathbf{E}(\omega_2)) + \dots \end{aligned} \quad (23)$$

$$\begin{aligned} \mathbf{P}^{(3)}(\omega) = \varepsilon_0 \chi^{(3)}(\omega = \omega_1 + \omega_2 + \omega_3; \omega_1, \omega_2, \omega_3) \cdots \mathbf{E}(\omega_1) \mathbf{E}(\omega_2) \mathbf{E} \\ \times (\omega_3) + \mathbf{P}'^{(3)}(\nabla \chi^{(3)}, \nabla \mathbf{E}(\omega_1), \nabla \mathbf{E}(\omega_2), \nabla \mathbf{E}(\omega_3)) + \dots, \end{aligned} \quad (24)$$

where ε_0 is the permittivity of vacuum, $\mathbf{E}(\omega_i)$ are the electric fields of the monochromatic components of the fundamental field with corresponding frequencies ω_i , and $\chi^{(n)}$ are the n th-order optical susceptibility tensors ($\chi^{(1)}$ is the tensor of linear optical susceptibility). The first terms in Eqs. (23) and (24) represent a bulk nonlinear response in an electric dipole approximation, while the second terms ($\mathbf{P}^{(2)}$ and $\mathbf{P}^{(3)}$), which include spatial derivatives of the fields and the nonlinear susceptibilities, represent nonlocal nonlinear response. Particularly, for the second-order nonlinear polarisation $\mathbf{P}^{(2)}(\omega)$, the latter includes magnetic dipolar and electric quadrupolar contributions.^[2]

3.1. Coherent Nonlinearities

Applying Eqs. (21)–(24) to the case of a monochromatic fundamental field, in the electric dipole approximation one can obtain $E(n\omega) \sim \chi^{(n)} E_{\text{loc}}^n(\omega)$, where $E(n\omega)$ is the field of the generated n th harmonic, and $E_{\text{loc}}(\omega)$ is the local fundamental field at the place where the harmonic is generated. This local field is characterized by a frequency and position dependent enhancement factor $L(\omega, \mathbf{r}) = E_{\text{loc}}(\omega, \mathbf{r})/E_0(\omega)$, where \mathbf{r} defines the position near (or in) the metal, which is related to the polarisability of the nanostructure.^[51] Thus, the effective nonlinear susceptibility can be significantly increased near the resonances of the plasmonic structure where the local electric field is enhanced. The generated nonlinear harmonic near-field as well as its radiation in the far-field, can be further enhanced if the electromagnetic resonances

and the related field enhancement $L(n\omega)$ are present at the generated frequency^[52] $E(n\omega) \sim \chi^{(n)} L(n\omega) L^n(\omega) E_0^n(\omega)$, which can be alternatively recast in terms of the effective nonlinear susceptibility $\chi_{eff}^{(n)} = \chi^{(n)} L(n\omega) L^n(\omega)$. This motivates the quest for the local electromagnetic field enhancement achievable with various nanostructures, and plasmonic nanostructures, providing very high local electromagnetic fields, are perfect candidates for the realisation of novel concepts for the augmentation of nonlinear effects.^[10] It should be noted, however, that in addition to the field enhancement, the spatial overlap of the modes at the fundamental and harmonic frequencies and their phase relations are important for efficient harmonic generation from nanostructures. A typical example is the phase-matching for SHG for propagating waves in bulk crystals (its analogue for localised modes^[53] is discussed below in Section 5.2).

3.2. Kerr-type Nonlinearities

The Kerr-type nonlinearity can be described by the changes of the permittivity of the material under the action of control light $E_c(\omega_c)$ and can be easily obtained from Eqs. (21) and (24) keeping the leading third-order nonlinear term:

$$\mathbf{P}(\omega) = \varepsilon_0 (\chi^{(1)} + \chi^{(3)} |E_c(\omega_c)|^2) \mathbf{E}(\omega). \quad (25)$$

Plasmonic excitations are extremely sensitive to the refractive index changes either in the metallic structure itself or in the surrounding material.^[54–56] This property can be exploited to control light with light, when a control beam induces the nonlinear change, modifying the plasmonic resonances and through them the propagation of a signal beam in waveguides or transmission or reflection of light from plasmonic nanostructures.

Under illumination with the control light, the third-order Kerr-type nonlinearity leads to the intensity-dependent refractive index $n(I) = n_0 + \gamma |E_{loc}(\omega_c)|^2$ and absorption $\alpha(I) = \alpha_0 + \beta |E_{loc}(\omega_c)|^2$, where n_0 and α_0 are the linear refractive index and absorption, respectively, $|E_{loc}(\omega_c)|^2$ is the intensity of the control light, and γ and β are the nonlinear refraction (sometime also called n_2) and absorption coefficients, respectively. The introduced changes in $n(I)$ and $\alpha(I)$ can be used to alter phase or absorption, respectively, of the signal light at a different frequency interacting with the nanostructure (the so-called cross-modulation). The strong beam can also influence itself via the same effects, leading to the so-called self-modulation. The local fields can be related to the polarisability of the plasmonic nanostructures in the same way as discussed above, and the effective nonlinear refraction and absorption coefficients can be introduced. The field enhancements inherent to plasmonic resonances, facilitate this nonlinear effect lowering the required control light intensities.

4. Plasmonic Metals as Nonlinear Materials

Free-electron plasma in metals and other plasmonic materials itself exhibits a strong nonlinear optical response due to complex dynamics of the electron gas in the inhomogeneous driving electromagnetic field. Free-electron nonlinearities provide one of the largest effective nonlinear susceptibilities and lead to a vast

family of intriguing nonlinear phenomena. Furthermore, metallic nonlinearities are inherently ultrafast allowing processing of optical signals at up to a femtosecond timescale, which is the second advantage of nonlinear plasmonics.

In terms of coherent nonlinearities, even-harmonic generation is forbidden in the dipolar approximation in centrosymmetric materials but significant surface contributions are observed. With the decrease of the nanostructure size, additional contributions from the bulk electron gas may arise due to inhomogeneous field and nonlocal effects. Unfortunately, even modern experimental data on the nonlinear response of metallic nanostructures from different sources are not always consistent because of the strong dependence on hardly controllable parameters, such as surface imperfections, nanostructure geometry variations, crystalline structure and other.

Kerr-type nonlinearities, which are predominately determined by heating of the electron gas (its energy redistribution in a conduction band), strongly depend on the energy supplied by the light to the electron plasma and, therefore, are strongly affected by the pulse energy and duration in terms of their values and time-response, varying over several orders of magnitude.^[57] They also may depend on the size of the particles and thickness of a metal layer due to modification of the electron scattering rate in nanostructures.^[58–60]

Both coherent and Kerr-type nonlinearities of metals may originate from several families of physical effects. One is related to the nonlinear dynamics of the free carriers plasma and is present in all spectral ranges.^[49,61,62] Another important contribution comes from the interband electronic excitation, when the driving field excites electrons from the valence band to conduction band of the metal.^[63] This nonlinearity is strong due to high efficiency of the absorption process but has a spectral range limited to the interband optical transitions. Recent experimental reports and theoretical approaches, relevant to those nonlinear mechanisms will be reviewed hereafter.

4.1. Perturbative Description of Coherent Nonlinearity of Metals

While Eqs. (1) and (2) can be directly used to describe the nonlinear response in the most general non-perturbative manner (as will be done in Section 6), a perturbative treatment allows to elucidate physics behind it. In order to solve the hydrodynamic equations in the case of relatively weak illumination intensities, small nonlinear corrections to the hydrodynamic variables can be assumed. Then, the hydrodynamic variables of the free-electron gas in Eqs. (1) and (2) can be represented as^[14,49]

$$n(\mathbf{r}, t) = n_0 + n_1(\mathbf{r}) e^{-i\omega t} + n_2(\mathbf{r}) e^{-2i\omega t} + \text{c.c.} + \dots, \quad (26)$$

$$\mathbf{v}(\mathbf{r}, t) = \mathbf{v}_1(\mathbf{r}) e^{-i\omega t} + \mathbf{v}_2(\mathbf{r}) e^{-2i\omega t} + \text{c.c.} + \dots, \quad (27)$$

where n_0 is the steady state nonperturbed density of the electron gas, $n_u(\mathbf{r})$ and $\mathbf{v}_u(\mathbf{r})$ ($u = 1, 2, \dots$) are the perturbative corrections to the electron density and velocity, respectively, appearing due to nonlinearity of the hydrodynamic equations. This translates into similar modifications of the polarisation $\mathbf{P}(\mathbf{r}, t)$ (Eq. (20)):

$$\mathbf{P}(\mathbf{r}, t) = \mathbf{P}_1(\mathbf{r}) e^{-i\omega t} + \mathbf{P}_2(\mathbf{r}) e^{-2i\omega t} + \text{c.c.} + \dots, \quad (28)$$

which act as a source for nonlinear harmonic generation:

$$\mathbf{E}(\mathbf{r}, t) = \mathbf{E}_1(\mathbf{r}) e^{-i\omega t} + \mathbf{E}_2(\mathbf{r}) e^{-2i\omega t} + \text{c.c.} + \dots, \quad (29)$$

$$\mathbf{H}(\mathbf{r}, t) = \mathbf{H}_1(\mathbf{r}) e^{-i\omega t} + \mathbf{H}_2(\mathbf{r}) e^{-2i\omega t} + \text{c.c.} + \dots. \quad (30)$$

Here $\mathbf{E}_i(\mathbf{r})$ and $\mathbf{H}_i(\mathbf{r})$ are the high-harmonic perturbative corrections to the local electric and magnetic fields, respectively. Expressing the hydrodynamic Eqs. (1) and (2) in terms of polarisation $\mathbf{P}(\mathbf{r}, t)$ ^[14,22,28] and expansions given by Eqs. (28)–(30), one obtains the fundamental and second harmonic polarisations taking the zero- and the first-order perturbation terms^[14,48]

$$\frac{v_F^2}{3} \nabla(\nabla \cdot \mathbf{P}_1) + (\omega^2 + i\omega\gamma) \mathbf{P}_1 = -\frac{n_0 e^2}{m} \mathbf{E}_1, \quad (31)$$

$$\frac{v_F^2}{3} \nabla(\nabla \cdot \mathbf{P}_2) + (\omega^2 + i\omega\gamma) \mathbf{P}_2 = -\frac{n_0 e^2}{m} \mathbf{E}_2 + \mathbf{S}_2^{NL}, \quad (32)$$

$$\begin{aligned} \mathbf{S}_2^{NL} = & \frac{e}{m} \mathbf{E}_1 (\nabla \cdot \mathbf{P}_1) + \frac{i\omega e}{m} \mathbf{P}_1 \times \mathbf{H}_1 - \frac{\omega^2}{n_0 e} [(\nabla \cdot \mathbf{P}_1) \mathbf{P}_1 \\ & + (\mathbf{P}_1 \cdot \nabla) \mathbf{P}_1] + \frac{2}{9} \frac{v_F^2}{n_0 e} (\nabla \cdot \mathbf{P}_1) \nabla(\nabla \cdot \mathbf{P}_1), \end{aligned} \quad (33)$$

which, coupled with the Maxwell's equations

$$\nabla \times \nabla \times \mathbf{E}_1 - \left(\frac{\omega}{c}\right)^2 \mathbf{E}_1 = \mu_0 \omega^2 \mathbf{P}_1, \quad (34)$$

$$\nabla \times \nabla \times \mathbf{E}_2 - \left(\frac{2\omega}{c}\right)^2 \mathbf{E}_2 = 4\mu_0 \omega^2 \mathbf{P}_2, \quad (35)$$

formulate the full set of equations for the calculation of the second harmonic response. The first term in Eq. (31) and (32) proportional to $v_F^2/3$ describes the linear nonlocal response for both first and second harmonic fields, while the components of \mathbf{S}_2^{NL} , which depend on the field derivatives, result in a nonlinear nonlocal response. Similar equations can be written for the higher perturbative orders, e.g., for third and higher harmonic generation.

In the case of small losses ($\gamma \ll \omega$), Eqs. (31)–(33) can be simplified to reveal the physical nature of the second harmonic nonlinear polarisation.^[14] Considering separately a thin sub-nanometre layer near metallic surface where the screening charge is accumulated (and, thus, the nonlocal effects are important) and the bulk of the metal, the second harmonic nonlinear source \mathbf{P}_2 can be presented as a sum of the contributions from a near-surface layer

$$\mathbf{P}_{2,\perp}^{surf} = \chi_{\perp\perp\perp}^{(2),surf} E_{1,\perp} E_{1,\perp}, \quad (36)$$

$$\mathbf{P}_{2,\parallel}^{surf} = \chi_{\parallel\parallel\perp}^{(2),surf} E_{1,\parallel} E_{1,\perp} \quad (37)$$

and bulk of the conductor

$$\mathbf{P}_2^{bulk} = \chi^{(2),bulk} \nabla(\mathbf{E}_1 \cdot \mathbf{E}_1), \quad (38)$$

where $\chi_{\perp\perp\perp}^{(2),surf}$ and $\chi_{\parallel\parallel\perp}^{(2),surf}$ are the surface second-order nonlinear susceptibilities, $\chi^{(2),bulk}$ is the bulk second-order nonlinear

susceptibility, $E_{1,\perp}$ and $E_{1,\parallel}$ are the components of the local fundamental field, normal and tangential to the surface, respectively. These terms were introduced by Rudnick and Stern^[64] using phenomenological parameters, which were estimated from the hydrodynamic approach with nonlocal linear response as^[14]

$$\left[\chi_{\perp\perp\perp}^{(2),surf}, \chi_{\parallel\parallel\perp}^{(2),surf}, \chi^{(2),bulk} \right] = -\frac{\epsilon \epsilon_0}{m\omega^2} (1 - \epsilon_D(\omega)) \left[\frac{a}{4}, -\frac{1}{2}, \frac{1}{8} \right], \quad (39)$$

where $\epsilon_D(\omega)$ is the permittivity of the metal in the simplest case considering $\epsilon_{core}(\omega) = 1$ and a is the coefficient defined by the solution of the hydrodynamic equations in the screening region. The exact value of the latter was not calculated in Ref. [14], though it was stated that $|a|$ is of the order of unity or less, but can be increased if the frequency of the second harmonic is close to the effective plasma frequency near the interface. The value of a can be determined from the comparison with the experiments. Expressions for surface and bulk nonlinear coefficients without any additional phenomenological parameters can be obtained neglecting nonlocality in the linear optical response.^[65,66] Even without the latter assumption, the second-order surface nonlinear currents can be expressed only in terms of bulk linear polarisation components, calculation of which do not require the resolution of the nonlocal equations.^[67] The bulk contribution can be also included into surface components, redefining them as $\chi_{\perp\perp\perp}^{(2),surf,eff} = \chi_{\perp\perp\perp}^{(2),surf} + \chi^{(2),bulk}/\epsilon(2\omega)$, $\chi_{\parallel\perp\perp}^{(2),surf,eff} = \chi^{(2),bulk}/\epsilon(2\omega)$ and $\chi_{\parallel\parallel\perp}^{(2),surf,eff} = \chi_{\parallel\parallel\perp}^{(2),surf}$.^[68] The above considerations were developed for a lossless hydrodynamic model. The additional term in the nonlinear susceptibility of isotropic and centrosymmetric bulk materials $\delta^{(2),bulk}(\mathbf{E}_1 \cdot \nabla)\mathbf{E}_1$ can be derived in the framework of the hydrodynamic model by including the Ohmic losses.^[66] Experimentally, the term $\delta^{(2),bulk}(\mathbf{E}_1 \cdot \nabla)\mathbf{E}_1$ was observed for metals using two-beam SHG experiments.^[68] It was shown that this term can be represented with surface electric and magnetic currents,^[69] which can be useful in the numerical treatment of the problem. The consideration of a lossy medium also leads to scaling of other nonlinear coefficients as γ/ω . In Ref. [66], the influence of the interband transitions was additionally taken into account, which can be important for matching the experimental observations.^[70]

4.2. Kerr Nonlinearity of Metals from the Hydrodynamic Model

Kerr nonlinearity coefficient can also be directly derived from the hydrodynamic equations. The physical interpretation of the effect is adopted from plasma physics and relies on the introduction of conservative ponderomotive potential. Introduction of the effective potential enables reformulation of the problem of collective interaction of the electron gas and adoption of a single electron description.^[71] A nonlocal ponderomotive (Gaponov–Miller) force^[72] can be derived from the electron motion in a non-uniform electromagnetic field and is given by

$$\mathbf{F}_{PM}(\mathbf{r}) = -\frac{1}{m} \left(\frac{e}{\omega}\right)^2 (\mathbf{E}(\mathbf{r}) \times (\nabla \times \mathbf{E}(\mathbf{r}))) + \mathbf{E}(\mathbf{r}) \cdot \nabla \mathbf{E}(\mathbf{r}). \quad (40)$$

The corresponding ponderomotive potential is then defined as

$$\Phi_{PM}(\mathbf{r}) = e^2 |\mathbf{E}(\mathbf{r})|^2 / 2m\omega^2. \quad (41)$$

As can be seen both from the above expression and from a detailed analysis of electron motion in a single particle representation, electrons will be pushed away from the region of the high field intensity. Consequently, electron concentration at the regions of high intensities will be reduced and, as the result, the real part of the local permittivity, which can be obtained in the framework of the Drude model, will become less negative. The process of the electron plasma dilution is balanced by restoring forces applied on an electron by surrounding carriers. The intensity-dependent permittivity then is given by^[50]

$$\begin{aligned} \varepsilon_{PM}(|\mathbf{E}(\mathbf{r})|^2) &= \varepsilon_D + \frac{3}{2} \left(\frac{\omega_p}{3\pi^2 \varepsilon_0 \hbar m e} \right)^{2/3} \left(\frac{e}{\omega} \right)^4 |\mathbf{E}(\mathbf{r})|^2 \\ &= \varepsilon_D + \chi_{PM} |\mathbf{E}(\mathbf{r})|^2, \end{aligned} \quad (42)$$

where $\varepsilon_D(\omega)$ is the permittivity of metal in the simplest case considering $\varepsilon_{core}(\omega) = 1$ and χ_{PM} is the nonlinear ponderomotive susceptibility. This Kerr-like coefficient is highly dispersive and for telecom wavelengths is on the order of $10^{-18} \text{ m}^2/\text{V}^2$, comparable with that of nonlinear glasses. Apart from Kerr solitons, this type of nonlinearity could lead to an intensity-dependent cutoff for SPP modes.^[50]

4.3. Kerr-type Nonlinearity of Metals: Thermal Response of Fermionic Gas

Light absorbed by metal either directly due to interband absorption or via excitation of surface plasmons followed by their fast (10 fs timescale) decay into hot electron excitations, leads in the first instance to modification of the electron distribution in the conduction band. The electron-electron scattering processes (10s–100s femtoseconds scale) that follow thermalise this nonequilibrium distribution establishing an excited state with the electron distribution at an elevated electron temperature. Electron-phonon scattering (on a picosecond timescale) converts this electron temperature into an increased material (lattice) temperature. The increase in the electron temperature can easily reach several thousands of Kelvins, but for the ultrashort pulses on femtosecond and picosecond timescales with reasonable energies, the material temperature changes are often negligible. During several hundreds of femtoseconds before the electron temperature increase is dissipated through the electron-phonon interaction, the optical properties of metal are dramatically changed, with both real and imaginary parts of the permittivity being modified as both are determined by the electron temperature.

Metal permittivity in this case can be represented within the random phase approximation that includes the dependence of the electron scattering on both electron (T_e) and lattice (T_L) temperatures.^[73,74] Within this approximation, the intensity-dependent permittivity can be described as the sum of the intraband permittivity and interband permittivity $\varepsilon_M = \varepsilon_{intra} + \varepsilon_{inter}$, which are dependent on the electron intraband (within the conduction band) and interband (in the case of Au, from the d -band

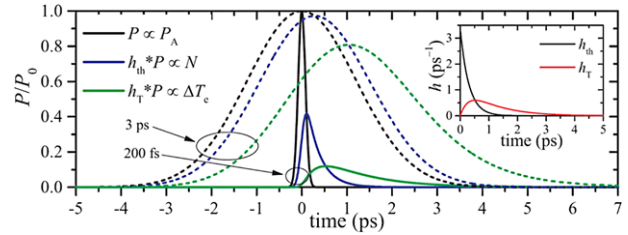


Figure 3. Transient electron dynamics in bulk gold for 200 fs (solid lines) and 3 ps incident Gaussian pulses (dashed lines). When pump power P is absorbed, giving rise to the absorbed power density P_A , the latter creates the nonthermalised electron density determined by the electron response function h_{th} (presented in the inset). Then, nonthermalised electrons are converted to the thermalised hot electrons described by the temperature elevated by ΔT_e with respect to the lattice temperature. P and ΔT_e are ultimately directly connected through the electron-temperature transient response function h_T (inset). Reproduced with permission.^[58] Copyright 2016, American Chemical Society.

to the conduction sp -band) transitions, respectively. The latter term can be reduced to a hydrodynamic Drude-like model (see Section 2.1) as

$$\varepsilon_{intra} = \varepsilon_\infty - \frac{\omega_p^2(T_L)}{\omega^2 + i\omega\gamma_{intra}(\omega, T_e, T_L)}, \quad (43)$$

where $\gamma_{intra}(\omega, T_e, T_L)$ related to both electron–electron and electron-phonon scattering, and the dependence of the bulk plasma frequency on the lattice temperature comes from possible thermal expansion of the nanostructure. The consideration of the interband transitions, which can be described using the random phase approximation^[75,76] and also results in the smearing of the Fermi distribution of the free carriers, is beyond the scope of this review devoted to free-electron nonlinearities. It should be noted that the nonlinear response related to the interband transitions also depends on electron and lattice temperatures.

The nonlinear response described by the two-temperature model depends on the excitation and probe pulse durations if they are comparable to the characteristic times of the electron relaxation processes.^[58] The excitation pulse is absorbed by the metal almost instantaneously so that the mean absorbed power density follows the shape of the incident pulse (Figure 3). The rise of the thermalised electron energy density is delayed by 100s of fs as the hot electrons release their energy and thermalise with a characteristic time determined by electron–electron and electron-phonon scattering rates. For short pulses (~ 100 fs), the rise of the electron temperature on the leading edge of the pulse is governed by the characteristic decay time of the nonthermalised electrons, while on the trailing edge it is governed by the characteristic relaxation time of the thermalised electrons. Then increased lattice temperatures dissipates on a multiple-picosecond scale until the ground state thermal equilibrium is reached. Instead, for long ($> \text{ps}$) pulses, the characteristic time scales of the electron dynamics become too fast for a pulse to experience any effects of the delayed responses, therefore, it experiences a quasi-instantaneous nonlinear response from the thermalised electrons. The interplay between the pulse duration and timescale of different relaxation processes determines for how long the pulse interact with the excited electron gas and the values of nonlinearity varies widely for

both $|\text{Re}(\chi^{(3)})|$ from $10^{-18} \text{ m}^2/\text{V}^2$ to $10^{-14} \text{ m}^2/\text{V}^2$ and $|\text{Im}(\chi^{(3)})|$ from $10^{-20} \text{ m}^2/\text{V}^2$ to $10^{-15} \text{ m}^2/\text{V}^2$, strongly decreasing for short excitation pulses.^[57] The relaxation time of the nonlinear changes depends on the energy supplied by light to the metal (the scattering rates and electron and lattice heat capacities are temperature dependent), as well as on the geometric and modal structure of the plasmonic system and thus can be controlled by nanostructuring, although in a limited range.^[77]

5. Harmonic Generation in Plasmonic Nanostructures: Perturbative Picture

5.1. Second Harmonic Generation

The investigation of second harmonic generation from nanostructures made from centrosymmetric metals^[78] started with studies of SHG from flat or curved surfaces^[14,49,64,65] and nanoparticles.^[79,80] The derived theory of the process related to the anharmonic response of the free electron gas based on the hydrodynamic model revealed both surface and bulk contributions. In the following studies, a substantial attention was devoted to determining the relative contribution of these terms for various nanostructures and finding the leading nonlinear mechanisms (Figure 4a).^[22,48,66–70,81–83] The surface contribution defined by $\chi_{\perp\perp\perp}^{surf}$ component is usually considered dominant, but the particular balance between various nonlinear sources is ultimately defined by the nanostructure geometry and material, as well as the fundamental and SHG frequencies. A typical SHG field map generated by a metallic nanowire with a square cross-section is shown in Figure 4b. Comparison with the experimental results for spherical nanoparticles shown that a direct application of nonlinear susceptibilities given by Eq. (39) with $a = 1$ produces only a rough fit to the observed data, but a good agreement can be achieved adjusting the relative impact of the terms in Eq. (39).^[70] Generally, for spherical nanoparticles, SHG was found to be a superposition of dipolar and quadrupolar contributions (both originating from the retardation effects),^[84–86] the importance of higher-order multipoles for larger particles was also predicted.^[83] Following the experimental observations, major mechanisms for the ordinary dipolar SHG contribution (with an induced SHG dipole along the polarisation direction of the illuminating light), forbidden for an ideally symmetric structure were proposed.^[87,88] Particularly, non-centrosymmetric shapes of the particles were invoked to explain the experimental results.^[89] Near-field SHG was studied with near-field excitation and detection, and was correlated with the surface topography.^[90,91] For a broad review of various experimental and theoretical studies of SHG from metallic nanostructures see Ref. [78].

The strategy of getting a qualitative increase of SHG from centrosymmetric metals by designing nanostructures of asymmetric geometrical shapes was identified.^[89,92] It was found that in order to make it efficient, the SHG engineering should rely on a certain selection rule, expressed in a semi-empirical criterion as^[93–97]

$$E_2 \propto \iint \chi_{\perp\perp\perp}^{(2),surf} (E_{1,\perp}^{mode})^2 E_{2,\perp}^{mode} dS, \quad (44)$$

where E_2 is the SHG field, $\chi_{\perp\perp\perp}^{(2),surf}$ is the surface nonlinear susceptibility tensor component, considered to be the dominant

SHG source, $E_{1,\perp}^{mode}$ and $E_{2,\perp}^{mode}$ are the components of the fields perpendicular to the metal-dielectric boundary for the modes at the fundamental and SH frequencies, respectively, and the integration is performed over the nanostructure surface. Particularly, this approach was used to optimise SHG from multiresonant coupled nanoantennas (Figure 4c).^[95] Exploiting the double-resonant condition (when the nanostructure has resonances both at the fundamental and SHG frequencies) and establishing a proper overlap between the modes, the SHG from a V-shape/rod structure was significantly enhanced (Figure 4d). The SHG efficiency can be further increased by obtaining a beneficial symmetry of the local fundamental field.^[98] This “selection” rule was also extended to the SHG studies from non-centrosymmetric metasurfaces. Other, more exotic scenarios, such as SHG from metamaterials with backward phase-matching were also considered.^[99]

SHG can also be enhanced through the excitation of magnetic-dipole resonances, as in, e.g., metamaterials based on the arrays of split-ring resonators (SRRs).^[100] SRRs have a magnetic-dipole response leading to the resonant enhancement of local magnetic fields, which results in a significant increase of the SHG polarisation related to the Lorenz nonlinear term in the hydrodynamic model ($-\epsilon \cdot \mathbf{v} \times \mathbf{H}$ term in Eq. (1)). Nevertheless, the SHG signals from the SRRs for both magnetic and electric dipoles have been measured with comparable values (Figure 4e).^[101] The time-domain numerical simulations based on the hydrodynamic model show that in addition to the Lorenz term, the convective acceleration term ($m \cdot \mathbf{v} \cdot \nabla \mathbf{v}$) plays a significant role in this type of nanostructures, accounting for 68% and 81% of the SHG power in SRRs and complimentary SRRs, respectively.^[101]

Finally, it is important to mention that SHG can be strongly affected by the roughness. In the case of metallic films, this was studied both experimentally and theoretically.^[102] The main features in the spatial distribution of SHG were discussed in terms of the roughness-assisted SPP generation as well as the LSP hot spots.^[103,104] For metallic nanostructures, it was numerically shown that small deviations from an ideal form due to asymmetry related to limited fabrication capabilities or surface roughness lead to significant changes in the radiated SHG, even if the linear response of the nanostructures is barely modified. From this point of view, SHG provides a very sensitive tool for the optical characterisation of plasmonic nano-objects and surfaces.^[104–106]

Third harmonic generation (THG) from metallic nanostructures was initially investigated on the examples of flat surfaces and spherical nanoparticles.^[107,108] The advantage of the plasmonic approach was used to demonstrate THG enhanced by the multipolar resonances either in individual metallic nanostructures^[109,110] or the resonant modes of 2D patterned metal surfaces.^[111–113] THG in metamaterials^[22] and other enhancement mechanisms, such as those involving interband transitions^[114] and phase-matching in a plasmonic waveguide^[115] were also considered.

5.2. Nonlinear Coupling of Localised Plasmonic Resonances of a Nanoparticle

The implementation of the perturbative hydrodynamic description allows the derivation of a fundamental criterion for

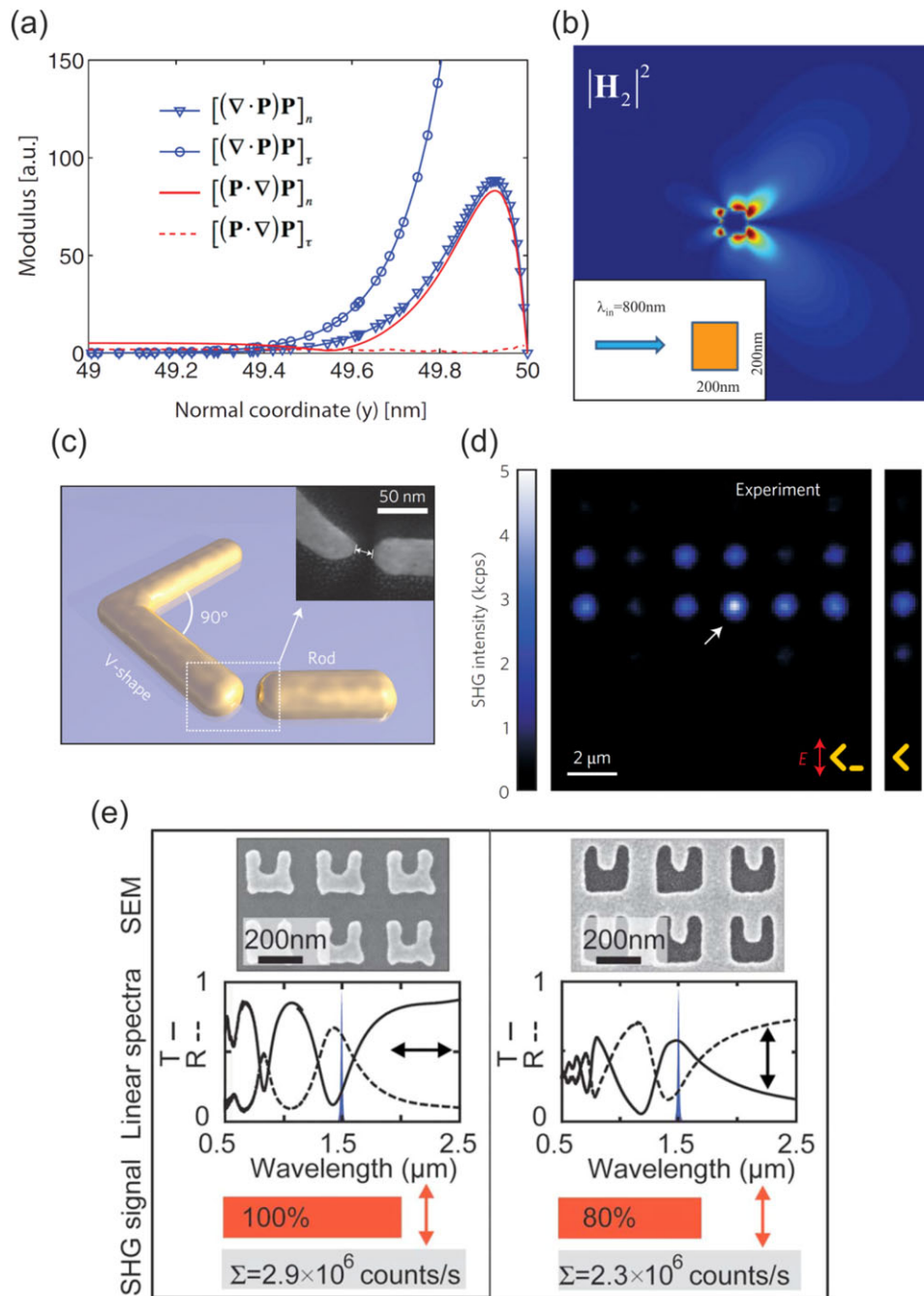


Figure 4. a) Relative contribution of various nonlinear sources in a sub-nanometre layer below the metal surface. Reproduced with permission.^[48] Copyright 2012, the American Physical Society. b) Snapshot of the SH field generated by a $200 \times 200 \text{ nm}^2$ metallic nanowire illuminated by a TM-polarised 20 fs pump pulse. Reproduced with permission.^[22] Copyright 2010, the American Physical Society. c) Metallic nanostructure for double-resonant SHG enhancement given by Eq. (44). d) SHG intensity map from an array of nanostructures shown in c): the rod length is varied from left to right with a 15 nm step from 80 nm to 155 nm, while the V-shaped half-arm length is varied from top to bottom with a 20 nm step from 140 nm to 240 nm. Reproduced with permission.^[95] Copyright 2015, Macmillan Publishers Limited. e) SEM images of split-ring resonators (left column) and complementary split ring resonators (openings in a metal film, right column), along with their linear transmission (T, solid lines) and reflection (R, dashed lines) spectra together with the values of the measured SHG signal; polarisations of the fundamental and SH waves are shown by the respective arrows). Adapted with permission.^[101] Copyright 2008, The Optical Society of America.

efficient generation of localised second harmonic modes at the nanoscale.^[53] In the most general case, an arbitrarily shaped metallic nanostructure is studied, and a plasmonic resonance with a field distribution

$$\mathbf{E}_1 = A_i^{(\omega)}(t) e^{-i\omega t} e^{-\gamma_i^{(\omega)} t} \mathbf{F}_i^{(\omega)}(\mathbf{r}) \quad (45)$$

is considered to be excited at a fundamental frequency ω . According to Eqs. (32) and (33), the fundamental field induces second-order nonlinear polarisation which excites localised SH modes

$$\mathbf{E}_2 = \sum_i A_i^{(2\omega)}(t) e^{-2i\omega t} e^{-\gamma_i^{(2\omega)} t} \mathbf{F}_i^{(2\omega)}(\mathbf{r}), \quad (46)$$

where $A_i(t)$ are the slowly varying (in comparison to ω) amplitudes of the multipoles, $\mathbf{F}_i(\mathbf{r})$ and γ_i are their normalised spatial mode distributions and damping coefficients, respectively. Substituting these expressions in Eq. (35) and using the SHG polarisation taken from Eqs. (31)–(33) for a lossless local case, one obtains the following expression for the evolution of the i -th localised SHG mode:

$$\frac{\partial A_i^{(2\omega)}(t)}{\partial t} = -i \frac{\epsilon}{m\omega\epsilon_0} \left\{ \frac{\oint \tau_i^{(2\omega)}(Q) [\sigma_1^{(\omega)}(Q)]^2 dS_Q}{\oint \tau_i^{(2\omega)}(Q) \sigma_i^{(2\omega)}(Q) dS_Q} \right\} e^{(\gamma_i^{(2\omega)} - 2\gamma_i^{(\omega)})t} \times \frac{S}{V} (A_1^{(\omega)})^2, \quad (47)$$

where σ and τ are the surface charge and surface dipole densities of the modes, S is the surface area of the nanostructure and V is its volume, the integration is performed over the nanostructure surface. The highest efficiency of the excitation will occur for the modes which maximise the overlap integral in the curly brackets of Eq. (47). Moreover, the multiplication factor of S/V shows explicitly the proportionality of the nonlinear process efficiency to the surface-area-to-volume ratio of the nanoparticle, emphasising the advantage of nanoscale geometries. Note that the nonlinear interaction here has a purely surface origin, supporting the experimental results reported in Ref. [87] and elsewhere.

The conversion efficiency of the nonlinear optical processes is usually linked to the local field enhancement since nonlinear polarisabilities are proportional to a certain power of the driving field. Here, a similar link can be made: high surface charge and dipole densities lead to high local electric fields. The “matching” integral in Eq. (47) may reach high values if these surface functions are spatially overlapped, meaning that the corresponding local fields of first and second harmonics also have a significant overlap. In particular, noncentrosymmetric particles can generate the second harmonic more efficiently. In our case, proper matching of parameters can maximise the spatial overlap integral in Eq. (47), resulting in more efficient SHG. The importance of matching was demonstrated on an example of localised mode coupling in an elliptical metallic nanoparticle. Equation (47) predicts a vanishing excitation efficiency for a second-harmonic dipole mode orthogonal to the fundamental dipole mode, since the surface integral of $\tau_i^{(2\omega)}(Q) [\sigma_1^{(\omega)}(Q)]^2$ is zero (Figure 5). At the same time, for the quadrupole mode this overlap is nonzero, meaning that it may indeed be excited if its resonance frequency

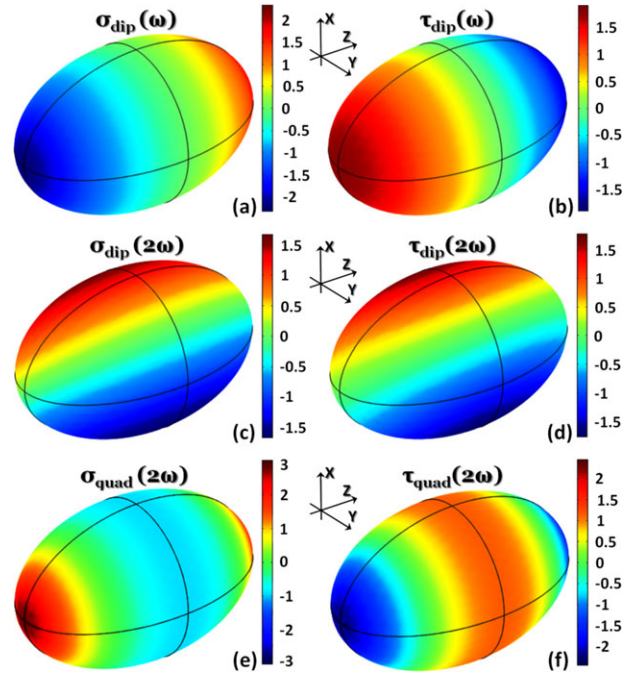


Figure 5. Distribution of surface charge density (left column) and the related surface dipole density (right column) for different plasmonic resonances of the spheroidal particle with the aspect ratio 1:1:1.6 for a,b) z-polarised dipolar resonance, c,d) x-polarised dipolar resonance, and e,f) z-polarised quadrupolar resonance. Reproduced with permission.^[53] Copyright 2012, The American Physical Society.

is twice that of the fundamental dipolar mode, which can be adjusted varying the ellipsoid geometrical parameters.

5.3. SHG from Coupled Nanostructures

Assembling plasmonic nanostructures in arrays has led to the development of artificial optical materials, metamaterials, with engineered optical properties beyond those that could be found in nature. In nonlinear optics, metamaterials present a new paradigm for a material platform providing nonlinear effects orders of magnitude higher than in naturally occurring media.^[74,116,117] Here, however, it appears another level of complexity. Both linear and nonlinear properties of such materials are defined not only by that of individual structures, ‘meta-atoms’, forming the metamaterial, but also by coupling among them (Figure 6a and b).^[118] For example, for the SRR-based metamaterials, the highest effective second-order nonlinearity is observed for an optimal separation between meta-atoms (Figure 6d) determined by the interplay of the effect of the decrease in the concentration of the meta-atoms for larger separations and the increase of the resonance damping for smaller separations due to the coupling effects among SRRs (Figure 6c). The above-mentioned double-resonance condition can also be realised in SRR-metamaterials, leading to the spectral dependence of SHG for a rectangular array of SRRs (Figure 6e) predicted from the hydrodynamic model (Figure 6g), which is in an excellent agreement with the experimental results (Figure 6f).^[118,119]

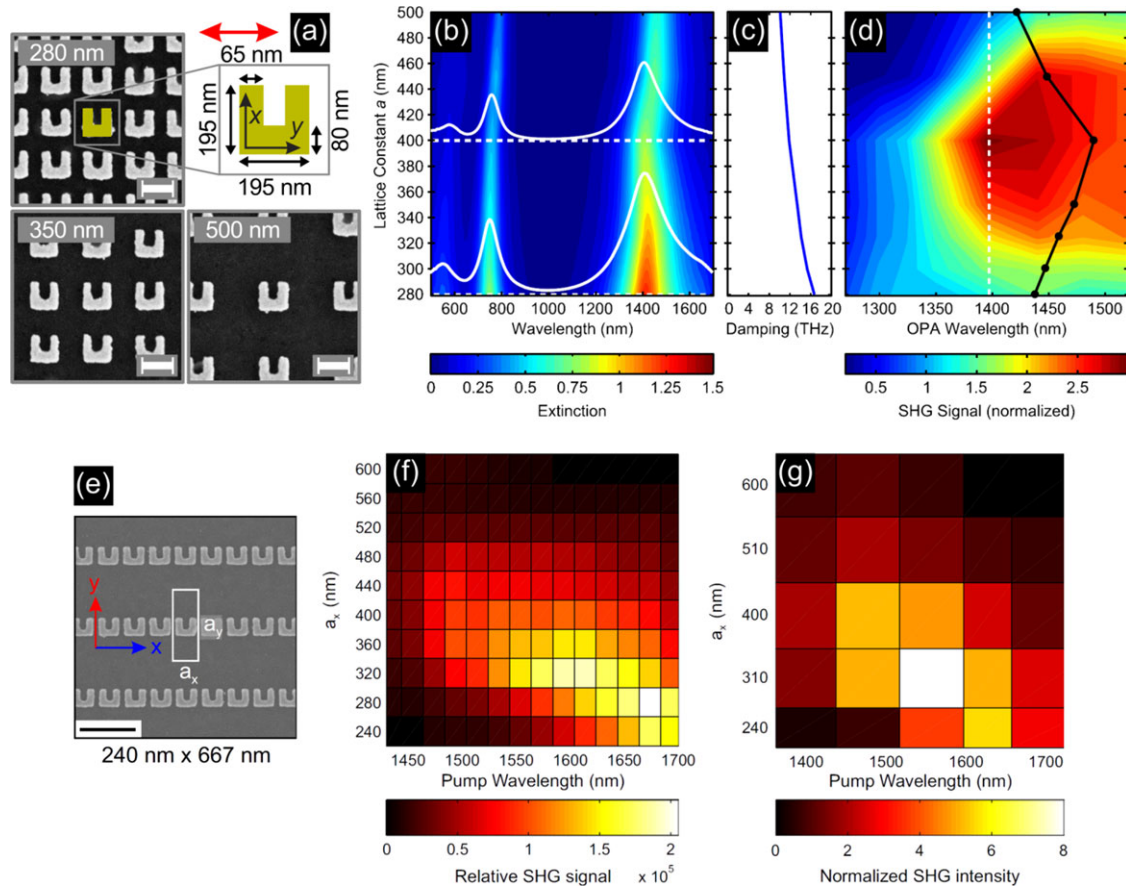


Figure 6. a) Geometry and SEM images of SRR square arrays with varied periodicity (red arrow indicates the polarisation of the incident light). b) Linear extinction spectra and c) linewidth of the fundamental resonance for different periodicity of the array. d) The dependence of the SHG intensity on the array period (the excitation wavelength is near the fundamental resonance). Adapted with permission.^[118] Copyright 2012, The American Physical Society. e) SEM image of a rectangular SRR array. f,g) Dependence of the SHG intensity on the fundamental wavelength and the horizontal lattice constant: (f) experimentally measured, (g) numerically calculated using the hydrodynamic model. Reproduced with permission.^[119] Copyright 2016, Springer.

In the other type of metamaterials, hyperbolic plasmonic metamaterials formed by arrays of vertically standing metallic nanorods, coupling between the nanorods results in the formation of waveguided modes which have significant influence on the SHG spectrum and efficiency, being an analogue of the double-resonant condition.^[120] The hyperbolic nature of the metamaterial provides an abundant spectrum of the waveguided modes with multiple resonances in infrared and visible spectral ranges. The sensitivity of the SHG response to the interaction between the meta-atoms can be used in SHG-based tomography for the ultrasensitive determination of a nano-object position within the metamaterial.^[121]

6. Harmonic Generation from Metallic Nanostructures in Non-perturbative Hydrodynamic Description

6.1. SHG and THG from Metallic Nanostructures in Non-perturbative Hydrodynamic Description

Although the perturbative models describe the dominating nonlinear processes in a very illustrative and physically clear way,

such analytic treatments are essentially restricted to studies of a predefined nonlinear effect relying on a set of electromagnetic modes in a limited number of geometries allowing analytical solutions. Also, such approaches have an inherent restriction in terms of the excitation powers for which the nonlinear variations can be considered as small perturbations. These conditions significantly limit the capabilities to describe, frequently inter-related, nonlinear processes from arbitrary geometries in strong fields, which can be achieved in plasmonics.

A non-perturbative numerical model for the investigation of nonlinear interactions of light with plasmonic nanostructures can be developed on the basis of a time-domain analysis to address the nonlinear dynamics of free electrons without any additional assumptions on the nature of the interaction, which provides the opportunity to explore the interplay between various nonlinear optical processes and a geometry of the nanostructures.^[101,122,123] Particularly, this approach gives an opportunity to explore simultaneously both bulk and surface contributions to nonlinear generation processes, as well as the efficiency of sideband generation, involving interplay between nonlinear effects. The time-domain implementation allows taking all these effects into account by coupling nonlinear

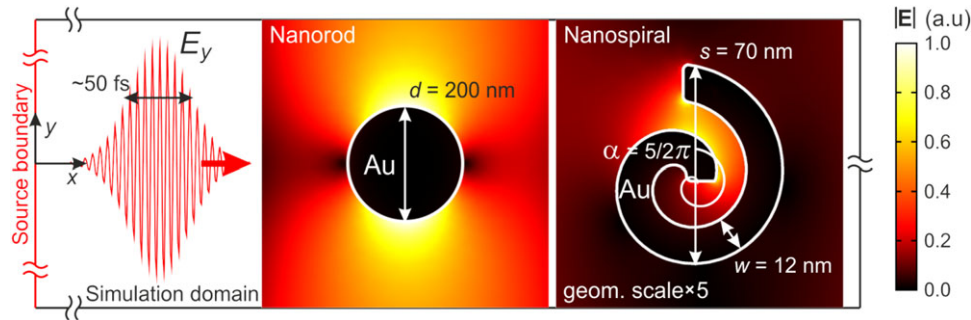


Figure 7. Layout of the time-domain numerical simulations: a ~ 50 fs vertically-polarised optical pulse with a central wavelength of 1500 nm is generated at a domain source boundary and illuminates a nanorod or an Archimedean nanospiral from the left. Fieldmaps show the normalised norm of the local electric field. Geometrical parameters of the nanorod and nanospiral are also shown. Reproduced with permission.^[123] Copyright 2016, Macmillan Publishers Limited.

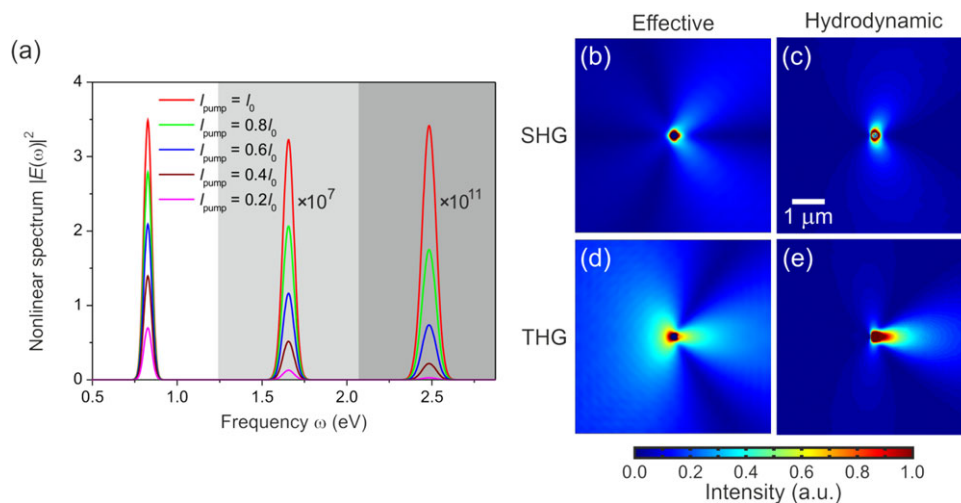


Figure 8. a) Nonlinear scattering spectra from an infinitely long Au cylinder of a 200 nm diameter simulated for a ~ 50 fs Gaussian excitation pulse. b, c) SHG and d, e) THG in (b, d) phenomenological and (c, e) microscopic hydrodynamic models. The colour scale is internal for each plot. Reproduced with permission.^[122] Copyright 2015, American Chemical Society.

hydrodynamic equations, which describe the behaviour of the electron plasma, with the Maxwell's equations to model the response to electromagnetic fields. This enables obtaining a universal, self-consistent numerical solution, free from any approximations, allowing for the investigation of nonlinear optical interactions with arbitrary spatially and temporally shaped optical pulses and opening unique opportunities to approach the description of realistic experimental scenarios. Furthermore, the developed formalism paves the way for the investigation of ultrafast dynamics in mesoscopic and nanoscopic systems with properties defined via microscopic degrees of freedom, which can be introduced in the permittivity model.

We compare the existing models to the non-perturbative hydrodynamic approach in the canonical case of metallic nanorods with a circular cross-section (Figures 7 and 8). The nonlinear scattering spectra obtained with the full model obviously shows both SH and TH contributions. Since the THG intensity grows with the third power of the fundamental intensity and the SHG does so with the second power of the fundamental intensity, the former shows a comparably faster growth with the excitation intensity (Figure 8a). In the case of the nanorods much smaller than

the wavelength, the SHG intensity scales with the diameter as $\propto d^4$,^[124] and provides 5 orders of magnitude difference in the SHG intensities from the nanorods with diameters $d = 200$ nm and $d = 12$ nm. Such drastic behaviour is the result of much smaller dipolar and quadrupolar moments (both of which are retardation-related) excited at the SH frequency for the smaller nanorod.

The SHG emission diagram from the nanorod has two radiation lobes pointing predominantly in the vertical (y -) direction and showing the sum of dipole and quadrupole radiation. In the chosen geometry, the main contribution to the SHG can be identified from the convective acceleration and the Lorenz force, having comparable contributions, while the quantum pressure effects were not observed. The relative contribution of the different terms may however differ depending on a particular geometry of the nanostructure. To compare this radiation pattern to that obtained from a frequency-domain phenomenological model, Figure 8c shows the SH radiation pattern evaluated using the approximate model polarisation $P_{2,\perp}^{surf} = \chi_{\perp\perp\perp}^{(2), surf} (E_{2,\perp})^2$.^[89] This assumes the perturbative regime with a nondepleted pump, relies on a quasi-Fourier separation of the harmonics, and makes the

explicit restrictive assumption that the interaction nature originates only from surface SH nonlinearity, particularly having only the component perpendicular to the surface. One can see the similarities of the phenomenological and non-perturbative models (cf. Figure 8b and c); however, the ratio between the dipolar and quadrupolar contributions is heavily distorted in the phenomenological model. Significant differences were also observed in the near-field of the nanorod in the third harmonic, compared with a phenomenological model based on bulk third-order susceptibility (Figure 8d and e). Since the latter assumes third-order susceptibility to be homogeneous across the nanorod, the differences between models may be indicative of position-sensitive effective third-order susceptibility arising in the hydrodynamic description. While higher harmonic generation is also described by the same non-perturbative hydrodynamic model, sufficient numerical accuracy of the simulations is needed to observe their presence.

6.2. Nonlocal and Resonantly-enhanced Nonlinear Phenomena

6.2.1. Coherent Nonlinear Effects and Nonlocality

Another very important feature of the hydrodynamic description is its inherent ability to describe nonlocal electromagnetic effects. The hydrodynamic nonlocality is a typical example of strong electron–electron interactions between quasi-free electrons of the metal plasma and was proven to describe a variety of phenomena governing the optical response of small plasmonic structures.^[38] (Please note that nonlocality discussed here has an electronic nature and is different from the nonlocality due to spatial dispersion in the effective permittivity of metamaterials,^[125] which is important for their Kerr-type nonlinear response discussed below). The relative contribution of nonlocal effects to nonlinear optical properties depends on the characteristic sizes of nanostructures.

The effect of the quantum pressure can be seen from comparison of nonlinear response of plasmonic nanorods of different diameters or Archimedean spiral shaped nanostructures (Figures 7 and 9a). Spirals have no symmetry of any kind and, hence, are good candidates for nonlinear optical interactions as they do not obey any geometrical selection rule.^[126] Initially, we consider a nonresonant excitation when the excitation frequency is lower than the lowest plasmonic resonances of both nanorods and nanospirals, in order to avoid the influence of the resonant effects. The unique ability to either include or exclude the quantum pressure term in the numerical model enables investigating the impact of nonlocality on the nonlinear generation. For large cylinders of 200 nm diameters (blue solid and dashed lines in Figure 9b), the nonlinear scattering intensity (with linear scattering field obtained in the local approximation subtracted) shows a clear signature of higher harmonics up to the 3rd order, though no significant impact from nonlocality. For smaller cylinders of 12 nm in size, the role of the quantum pressure is more significant. At the length scale of few nm ($r = 6$ nm in our case), which is smaller than the mean free pass of electrons and becomes comparable with the radius of nonlocality related to the electron Fermi wavelength (~ 0.5 nm), the nonlocal response starts playing an important role in the nonlinear scattering of the nanos-

tructures. While the structure of the local and nonlocal spectra remains almost unchanged up to the 3rd harmonic (dashed and solid green lines in Figure 9b, respectively), the intensity between integer harmonics in the nonlocal case is tremendously enhanced compared with the local counterpart. The effect of nonlocality, however, is much more pronounced in the case of the spiral nanostructure (red lines in Figure 9b). For both nanospirals and nanospheres, the enhancement rises linearly with the excitation intensity and is probably related to the nonlocality-induced change in the nanostructures' linear response over the wide spectrum of the excitation pulse and frequency mixing of generated harmonics.

6.2.2. Resonant Coherent Nonlinear Response

Resonant properties of plasmonic nanostructures give them a decisive advantage for the generation of high intensity nonlinear signals at the nanoscale. When the frequency of the excitation light matches the frequency of the plasmonic mode, the latter is resonantly excited, leading to pronounced enhancement of the local fields. The enhancement of the associated nonlinear signal is even more dramatic, since its intensity is proportional to higher powers of the excitation intensity, given by the order of the interaction. From this point of view, nanospirals present a very robust and efficient class of nanostructures, offering well-defined narrow resonances (Figure 9a), which can be easily adjusted to a given frequency.

In the case of the spiral with geometrical parameters considered above, the local fields are enhanced by factors of ~ 35 and 50 for the first (1.2 eV) and second (2.9 eV) plasmonic resonances, respectively (Figure 9a). Taking advantage of the flexibility of the spiral geometry, the lowest plasmonic resonance of the nanospiral was matched to the frequency of the pump (1550 nm or 0.83 eV) by increasing the angle of the spiral (and consequently its length) to the value $\alpha = 1.03 \cdot 3\pi$ slightly above 3π (Figure 9c and d). Such optimised structure now provides the highest field enhancement at the first resonance, rather than at the second one.

As one can see by comparing the nonlinear responses of the resonant spiral to the nonresonant spiral and the nanorod ($d = 200$ nm), the intensity of the SHG signal increased by >5 and 4 orders of magnitude, respectively, with a further several orders of magnitude increase throughout the nonlinear supercontinuum spectrum (Figure 9e). Comparing with the nonlinear spectrum of a nanorod with a diameter equal to the nanospiral arm width ($d = 12$ nm), the difference is even more striking with more than a 9 orders of magnitude increase of the SHG intensity and a 8 to 3 orders of magnitude increase of higher-harmonic intensities. Such striking difference highlights the importance of the resonant effects for enhancing the nonlinear interactions as well as the importance of topology of the nanostructure: the surface area and volume of the considered nanospirals are different by only one order of magnitude: 10 and 20 times, respectively. The effective second-order nonlinear susceptibility of a nanospiral can be estimated to be about $\chi^{(2)} = 600$ pm V⁻¹ considering a spiral with the same geometrical parameters made from a uniform material with $\chi^{(2)}$ that

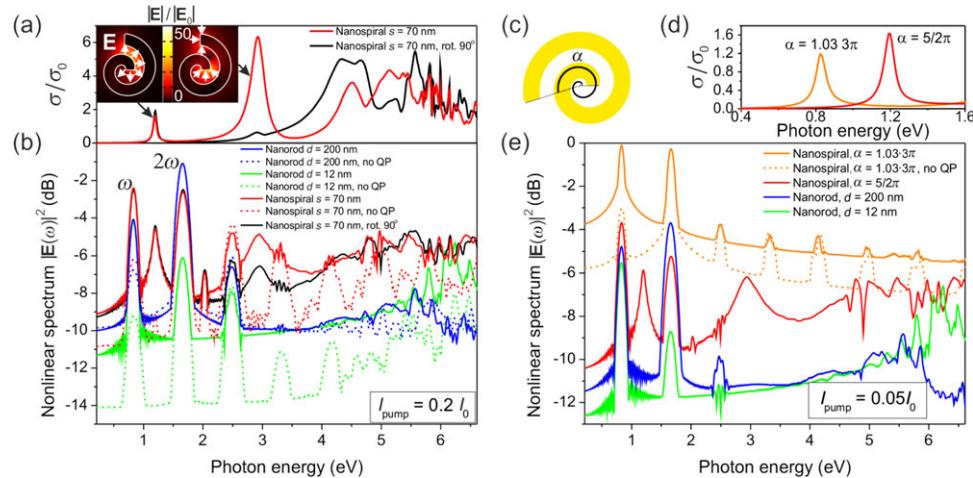


Figure 9. a) Extinction cross-section spectra of an Archimedean nanospiral normalised to its overall geometrical cross-section modelled with linear frequency-domain numerical simulations. The insets show electric field enhancement maps $|E|/|E_0|$ for the first two nanospiral resonances with respect to the norm of the electric field of the incident wave. The white arrows show the direction of the local electric field. b) Nonlinear scattering spectra of the nanospirals and nanorods of various geometrical parameters for a ~ 50 fs Gaussian excitation pulse: solid and dashed lines correspond to the hydrodynamic model with and without the quantum pressure term, respectively. c) Schematic of the nanospiral indicating the angle α , defining the positions of the nanospiral resonances. d) Spectral dependences of the extinction cross-section of the nanospirals with $\alpha = 5/2 \cdot \pi$ and $\alpha = 1.03 \cdot 3\pi$ normalised to their overall geometrical cross-section ($s = 70$ nm and $w = 12$ nm). e) Nonlinear scattering spectra of the nanospirals with $\alpha = 1.03 \cdot 3\pi$ (having the resonance at the fundamental frequency) and $\alpha = 5/2 \cdot \pi$ and the nanorods with $d = 200$ nm and $d = 12$ nm. Reproduced with permission.^[123] Copyright 2016, Macmillan Publishers Limited.

produces the same overall SHG flux. This effective susceptibility is 20 times higher than that of lithium niobate, a commonly used nonlinear material^[127]. This value for the simulated nanostructures in the absence of nonlocal effects is consistent with the experimentally observed values of the effective second-order susceptibility of metallic nanostructures of 10 pm V^{-1} ^[126] and 3.2 pm V^{-1} ^[128], taking into account the differences in the local field enhancements and the surface areas. The SHG enhancement is robust with respect to geometrical scaling under the resonant excitation of the fundamental nanospiral mode which size-dependent spectral position can be matched to the fundamental wavelength by varying α . The SHG intensity from a twice larger nanospiral increases by the factor of ~ 1.4 in accordance with a similar increase of the surface area. Also, it was demonstrated that the nature of the fundamental resonance remains the same in the most common experimental situation when the light is incident from the top at a nanospiral of finite thickness on a substrate. The resonances exhibit similar field distributions and field enhancement values (this is not surprising for the nanoscale structure size with nonessential retardation effects), which leads to the same nonlinear phenomena as discussed above.

7. Kerr-type Nonlinearity and Ultrafast Nonlinear Plasmonics

7.1. Controlling Light with Light

In the presence of Kerr-nonlinearity (Eq. (25)), the transmission, reflection or absorption of light at a given wavelength (signal light) can be affected by the presence of strong control light, which induces the nonlinear permittivity changes (the so-called

cross-modulation). The latter signal can be either free-space light or any waveguided mode, including SPP. Alternatively, in self-modulation realisation, light can experience self-induced nonlinear propagation phenomena, if its intensity is strong enough to induce nonlinear Kerr-effects. The latter can manifest themselves as nonlinear refraction, when refractive index of the material is changed or nonlinear absorption or transmission if the imaginary part of the refractive index is affected.

The Kerr nonlinearity of metals is very fast and, in different regimes, its time response ranges from tens of fs to few ps, depending on which electron plasma relaxation processes can be accessed with the particular nanostructure and excitation duration and power.^[129–131] The use of plasmonic structures for all-optical modulation, switching and achieving optically tunable photonic properties relies on enhancing Kerr-type nonlinearities of an adjacent dielectric or a metal itself and utilising the modified refractive index via changes in scattering associated with localised surface plasmons or guiding properties of the structures relying on surface plasmon polaritons.

Plasmonic-enhanced interaction of light with light can be achieved with metal nanoparticles themselves^[132–134] or bulk materials (e.g., nonlinear polymers) doped with them.^[63,135,136] The effective third-order susceptibility is determined by the field enhancement at the control light wavelength. The excitation of such composites at the wavelength of the nanoparticle LSP resonance ($\omega_c = \omega_{\text{LSP}}$) leads to an increase in the effective nonlinear susceptibility compared to an off-resonance excitation as described in Section 3.2. Under the control illumination, the local changes of the dielectric constant of the materials are induced resulting, in turn, in the changes of the resonances of the metal nanostructures and, thus, signal light propagation. Under such conditions, resonances either shift (phase modulation), if the real part of the refractive index is affected, or the resonances are suppressed

(absorption modulation), if the imaginary part is strongly modified. This approach can be used in both self-modulation mode, when the propagation of light is influenced by the changes due to its own intensity, or cross-modulation mode, when light at one frequency (control) influences the propagation of the light at a different frequency (signal).

Recently, specifically designed plasmonic nanoantenna resonances have been used to control light scattering using the ITO free-carrier nonlinearity in the picoseconds regime.^[137] The Kerr-type nonlinear change was used to realise ultrafast all-optical modulation of the transmission through plasmonic nanostructured surfaces,^[138] metasurfaces,^[139] gratings,^[140] nanoparticle arrays,^[141] SPP crystals^[142,143], plasmonic cavities^[144] and individual nanostructures.^[134] Applications of plasmonically-enhanced nonlinearities for pulse polarisation control^[145] and shaping^[146] were also proposed.

Concurrently, if surface plasmon polaritons are chosen to be signal carriers, the high sensitivity of their dispersion to the geometrical and material parameters of a structured surface where they propagate^[4] brings a viable solution to the problem of on which all-optical control. In this scheme, minute changes induced in the refractive index of a nonlinear material placed on the metal surface or in metal itself would significantly influence the SPP propagation. In order to optically modulate and switch SPP signals in a waveguiding geometry, two approaches are possible, based on the control light induced changes of the real and/or imaginary part of the permittivity of the materials. The latter has been explored based on a control light induced absorption modulation due to the changes of the imaginary part of the permittivity of the plasmonic metal^[142,147] as well the dielectric forming the plasmonic waveguide.^[148,149] The variation of the real part of the metal influences the propagation of the SPP modes via modification of their phase velocity and thus, can be used in various phase-sensitive configurations such as Mach-Zehnder interferometers (MZI) or waveguide-ring resonators (WRR).^[150–153] In plasmonic crystals, the free-electron nonlinearity of Au has been used to control the SPP excitation with sub-ps response times determined by the electron relaxation.^[142,143]

Finally, not only linear, but also nonlinear properties of plasmonic nanostructures can be controlled via Kerr nonlinearity in metal on an ultra-fast timescale. The all-optical control of SHG and THG from cut-disk-based metasurfaces was experimentally realised showing significant variation of SHG intensity (up to 20%) with control light illumination (Figure 10).^[154]

7.2. Nonlinear Plasmonic Metamaterials

Plasmonic metamaterials provide additional opportunities for utilising nonlinear effects for all-optical switching, since not only the plasmonic resonances of individual nanostructures but the interaction between them in the metamaterial can be influenced. Optical properties of metamaterials are determined by plasmonic resonances of the constituents, e.g., SRRs or nanorods, as well as the electromagnetic coupling between them.^[155] The nonlinearity of plasmonic SRRs in the metamaterials has been used to achieve very fast modulation times under 100 fs using the intrinsic nonlinearity of gold under two-photon excitation.^[156] In

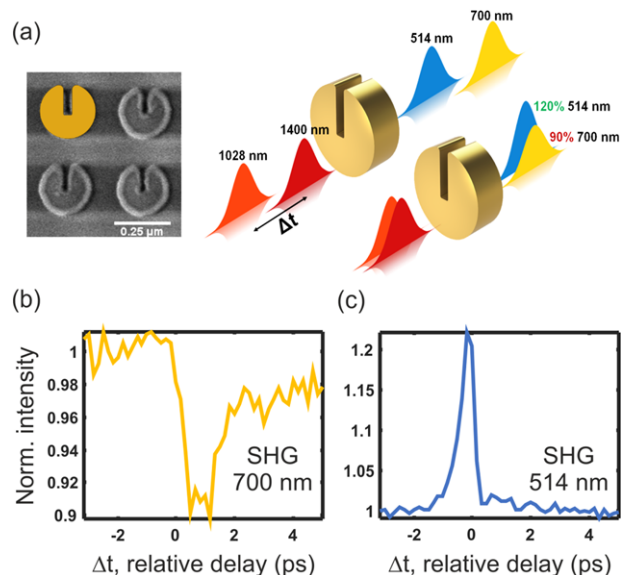


Figure 10. a) Sketch of the experimental setup for ultrafast optical modulation measurements of second- and third-harmonic generation from cut-disk-based metasurfaces. Inset shows an SEM (scanning electron microscopy) image of the metasurface with the marked unit cell metallic element. Second harmonic modulation signal from b) pump and c) probe pulses. Reproduced with permission.^[154] Copyright 2016, American Chemical Society.

contrast to plasmonic crystals, metamaterials have characteristic sizes of the elements and separations between them much smaller than the operating wavelength, so that they can be described by introducing effective medium parameters through the averaging over many periods. While such effective medium approach describes the linear optical properties of metamaterials (reflection, transmission and absorption) well, it should be applied to treatment of nonlinear optical properties with caution as it does not take into account the local fields inside the metamaterial composites which can vary significantly.^[157] (For the same reason, it also is not applicable for the description of the Purcell effect for the emitters inside the metamaterial.^[158,159]) The extension of the effective medium model taking into account local field variation via spatial-dispersion effects may alleviate this problem in some cases, in particular in the case of hyperbolic metamaterials.^[158,160–162]

Plasmonic metamaterials also provide an opportunity to develop a new approach to the enhancement of nonlinearity utilising the effects which arise in the epsilon-near-zero (ENZ) regime,^[160,163] when the real part of the effective medium permittivity of the metamaterial is close to zero. In this case, nonlocal spatial dispersion effects become important. In particular, this happens in a metamaterial formed by an array of vertically aligned metallic nanorods (Figure 11a) for the permittivity component in the direction parallel to their axes. The nonlocal effects depend strongly on the losses in the system and can be significantly modified by controlling loss in the Au nanorods. The modulation is based on nonlinear response of Au under the interband excitation, leading to the significant changes of $\text{Im}(\epsilon)$ of Au, which results in very strong changes of the metamaterial transmission due to modification of the nonlocal response.

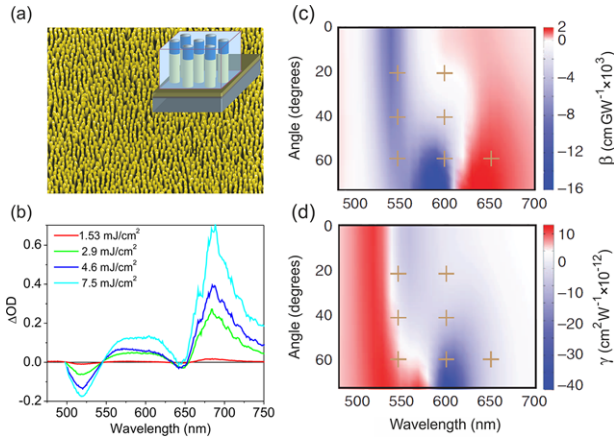


Figure 11. a) Optical metamaterial formed by an array of gold nanorods (diameter 20 nm, length 400 nm, an average inter-rod separation 70 nm). b) Measured transient extinction spectra of the nanorod metamaterial for various pump fluencies. Reproduced with permission.^[163] Copyright 2011, Macmillan Publishers Limited. c) Nonlinear absorption and d) nonlinear refraction coefficients for the nanorod array metamaterial calculated using a finite element method for different angles of incidence and wavelengths. Reproduced with permission.^[74] Copyright 2016, Macmillan Publishers Limited.

The transmission changes of up to 80% with a sub-picosecond response time have been observed for nanorod-based metamaterials (Figure 11b). To achieve this performance in $100 \times 100 \text{ nm}^2$ devices, 10 fJ pulses are sufficient.^[163] Such metamaterials can also be integrated in nanophotonic waveguides, e.g., Si waveguides, to provide very efficient all-optical modulation and switching of the guided signals using all-optically controlled coupling between waveguide and metamaterial modes.^[164] The operation performance of such metamaterial-based modulator is comparable with other integrated all-optical counterparts.^[165]

The strong Kerr nonlinearity of metals is significantly restricted to the spectral range of the interband electronic transitions where efficient excitation of electrons to the conduction band takes place, leading to the strongest nonlinear response. This nonlinearity becomes weaker at frequencies away from the interband absorption, limiting its usefulness to the (near) ultraviolet spectral range of the control light wavelength. On the other hand, the strong absorption near the interband resonance, in many cases, prohibits useful applications when the signal light, which may be controlled by this nonlinearity, overlaps with this spectral range. If, however, Au nanostructures form a hyperbolic-type metamaterial, the nonlinearity near the effective plasma frequency^[166] of the metamaterial where the ENZ-regime is achieved, is strongly enhanced.^[163] Not only the enhanced nonlinear response but the sign of the nonlinearity at the required wavelength can be engineered by changing the geometrical parameters of the nanorod metamaterial.^[74]

The z-scan measurements allow the direct determination of the nonlinear refraction, γ , and nonlinear absorption, β , coefficients related to an intensity-dependent, complex-valued effective refractive index of the metamaterial $\tilde{n} = n + i\alpha/(2k_0)$, k_0 being the light wave vector and $n(I) = n_0 + \gamma I$ and $\alpha(I) = \alpha_0 + \beta I$, where n_0 and α_0 are the linear refractive index and the absorption, respectively, and I is the intensity of the incident light. As a con-

sequence of the metamaterial's anisotropy, the retrieved effective values of nonlinear refraction $\gamma(\theta)$ and nonlinear absorption $\beta(\theta)$ coefficients for a specific angle of incidence θ_i that can be related to the components of the effective third-order nonlinearity tensor of the anisotropic metamaterial as^[74]

$$\varepsilon_{eff}(\theta_i) \approx \varepsilon_{eff}^0(\theta_i) + 3\varepsilon_s \sin^2 \theta_i \left[\chi_{xxxzz}^{(3)} + A(\theta_i) \frac{\chi_{zzzz}^{(3)}}{\varepsilon_{zz}^0} \right] |E_0|^2, \quad (48)$$

where $A(\theta_i) = 1 - \frac{\varepsilon_{eff}^0(\theta_i)}{\varepsilon_{xx}^0} - \frac{\varepsilon_s \sin^2 \theta_i}{\varepsilon_{xx}^0} \frac{\chi_{xxxzz}^{(3)} - \chi_{zzzz}^{(3)}}{\chi_{zzzz}^{(3)}}$ is the angle-dependent but nonresonant term, ε_{xx}^0 and ε_{zz}^0 are the components of an effective linear permittivity tensor of the metamaterial, $\chi_{xxxzz}^{(3)}$ and $\chi_{zzzz}^{(3)}$ are the components of a third-order nonlinear susceptibility tensor, dominant for the transverse magnetic polarized (TM) light, ε_s is the permittivity of the medium adjacent to the metamaterial from the side of the incident light, and $|E_0|$ is the incident electric field amplitude. One can see that near the effective plasma frequency when ε_{zz}^0 is close to zero, the effective nonlinearity is greatly enhanced.

The largest nonlinearity was experimentally measured in these conditions corresponds to $\gamma \approx -2.4 \times 10^{-11} \text{ cm}^2 \text{ W}^{-1}$ and $\beta \approx -9967 \text{ cm GW}^{-1}$. At the same wavelengths, $|\gamma|$ and $|\beta|$ of the nanorod metamaterial are approximately 20 and 100 times larger than those measured for a smooth Au film.^[57] Surprisingly, the maximum value obtained for γ and β for the metamaterial away from Au interband transitions is larger than the maximum values measured for a smooth gold film close to the interband transition where they usually are the highest. While in the studied range of frequencies, the nonlinearity of smooth Au is always positive (induced absorption and focusing nonlinearity), the Au nanorod metamaterial can provide either induced absorption, transparency, focusing or defocusing nonlinearity, depending on the combination of light wavelength and angle of incidence (Figure 11c and d). Thus, not only the strength but also the sign of the nonlinearity can be designed with plasmonic metamaterials.

The wavelength at which the strongest nonlinearity is observed can be engineered and pre-defined at the fabrication stage by setting the proper geometrical structure with the same constituent materials. Therefore, an artificial optical material with a strong nonlinear response can be realised at the wavelengths where the constituent materials have negligible nonlinearity. As an example, in Ref. [74] a nonlinear Au nanorod metamaterial was designed for the telecommunication spectral range where Au has a negligible nonlinear response.

It should be noted that the condition on the nonlinearity enhancement in the ENZ regime similar to that given by Eq. (48) is also valid for conventional plasmonic materials. Very strong nonlinearity was observed for thin ITO films at the plasma frequency in the telecommunication spectral range^[167] as well as using semiconductor plasmonic nanocrystals.^[168]

8. Nonlinear Surface Plasmon Polaritons

Ultrafast plasmonic Kerr nonlinearity can substantially influence the propagation of the SPP modes at the metal/dielectric interface, particularly in the case of dielectrics lacking a strong nonlinear response.^[169] For example, it was shown both theoretically

and experimentally that in this case SPPs experience prominent self-induced absorption.^[170] Nonlinearity may lead to completely unexpected behaviour of SPPs. In a linear case, when considering nonmagnetic media, SPPs are always TM-polarised surface waves. However, if the Kerr-type nonlinearity is introduced, transverse electric (TE)-polarised nonlinear surface waves may exist at the interface between a nonlinear dielectric and a linear metal or a linear dielectric and a nonlinear metal.^[8] The former case has more stringent requirements on nonlinearity of the dielectric (it should be defocusing and stronger than the nonlinearity of metal), while the latter case can always be achieved considering free-carrier nonlinearity of metals under strong enough intensity of the exciting light. Propagation of high-intensity SPPs at the interfaces bounded by a nonlinear medium also results in other interesting phenomena such as self-phase modulation^[171] and soliton-like behaviour of plasmonic waves. In this section, several nonlinear phenomena influencing the propagation of SPPs with the nonlinearity stemming either from the metal or the dielectric components of a plasmonic waveguide will be discussed.

8.1. Nonlinear SPP Modes due to Ponderomotive Nonlinearity

General nonlinear phenomena in planar SPP waveguides were extensively studied and various combinations of the nonlinearities were considered.^[172] The propagation of SPP modes is affected by the third-order nonlinearity even in the most basic SPP supporting structure: a single metal–dielectric interface.^[50] At the wavelengths longer than the inter-band transitions range, the third-order nonlinearity can be attributed to the previously discussed ponderomotive forces. This dynamic phenomenon, having a direct counterpart in classical plasmas, leads to repelling of electrons from the region of the high field intensity. As the result, the corresponding nonlinear effect is related to electron depletion in the high-intensity regions that are located just at the metal–air boundary. The linear effective index of the SPP mode is given by $\sqrt{(\epsilon_m + \epsilon_d)/\epsilon_m \epsilon_d}$, where ϵ_m and ϵ_d are the permittivities of the metal and dielectric media, respectively. As a result of the carriers' depletion next to the guiding boundary, the negative metal permittivity near the interface becomes less negative, and may approach a critical value of $\epsilon_m = -\epsilon_d$. At this condition, the SPP mode approaches its cut-off. For light intensity corresponding to this critical value, the intensity-induced modal reshaping results in equal, but opposite, power flows in the metal and the dielectric. The corresponding SPP intensity-dependent nonlinear dispersion relations show the intensity dependent cut-off wavelengths for the nonlinear SPP modes (Figure 12).

8.2. Cascaded Plasmon-solitons due to Second-order Nonlinearity

Second-order nonlinearity can lead to spatial soliton wave formation via the effect of second-harmonic generation, as was theoretically predicted^[173] and experimentally demonstrated in, e.g., potassium titanyl phosphate (KTP) crystals^[174] and planar LiNbO₃ waveguides.^[175] The principle behind such spatial solitons is the collinear propagation of two beams, one at fundamen-

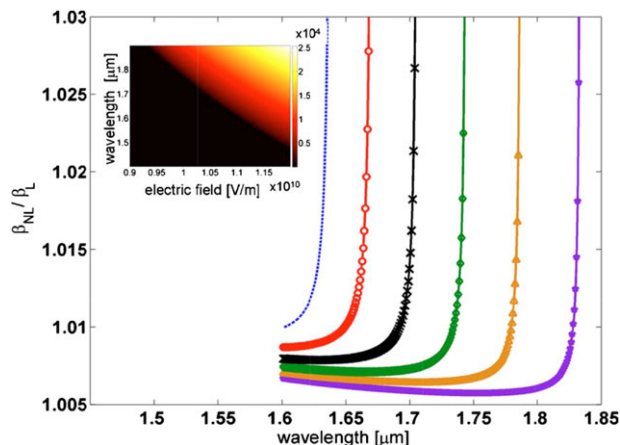


Figure 12. Dispersion of a single-surface nonlinear SPP on air–gold interface for different interface electric field amplitudes: (dashed blue line) 12 GV/m, (red line with circles) 11.5 GV/m, (black line with crosses) 11 GV/m, (green line with diamonds) 10.5 GV/m, (brown line with triangles) 10 GV/m, (purple line with stars) 9.5 GV/m. The inset shows the nonlinear effective index normalised by the linear one as a function of the wavelength and the field amplitude. Reproduced with permission.^[50] Copyright 2010, The Optical Society of America.

tal and another at the second-harmonic frequency. These beams exchange their energies via the second-order polarisability, which coined the term ‘cascaded $\chi^{(2)}$ solitons’. Such an exchange provides the maximum phase delay at the region of high intensity, resulting in self-focusing. This nonlinear phenomenon provides many opportunities for applications and fundamental studies of solitonic effects.^[176]

Here, following Ref. [177], we illustrate the concept of cascaded $\chi^{(2)}$ SPPs propagating at the interface between a linear dielectric and a metal with the nonlinearity described by the hydrodynamic model. Two co-propagating SPP beams, one at ω , another at 2ω , are considered to be nonlinearly coupled through the nonlinear polarisation of the metal.

SPP modes are strongly confined to the metal–dielectric interface where the nonlinear interactions take place. The mismatch between the effective refractive indices of the fundamental and the second-harmonic beams, reflecting the dispersion of the SPP waves and determining the essential phase relations between the waves, should be taken into account. The finite propagation distance of SPPs, which is determined by Ohmic losses in the metal plays a significant role in the formation of this type of solitons.

The SPP beams at the fundamental and second-harmonic frequencies propagate collinearly along the z -axis with transverse field profiles described by Gaussian distributions. Comparing the evolution of the SPP profiles during the propagation in linear and nonlinear regimes, the formation of the solitons can be observed (Figure 13). The intensity distributions $|E_{1,2x}|^2$ obtained in the linear (uncoupled) regime show typical diffraction-governed propagation for both fundamental and second-harmonic SPP beams (Figure 13a and d). When the SPP intensity is gradually increased so that the nonlinear interaction is introduced, the intensity distributions become deviating from that in the linear propagation regime. The observed intensity fringes are defined by the mismatch between the SPP effective indices at the two

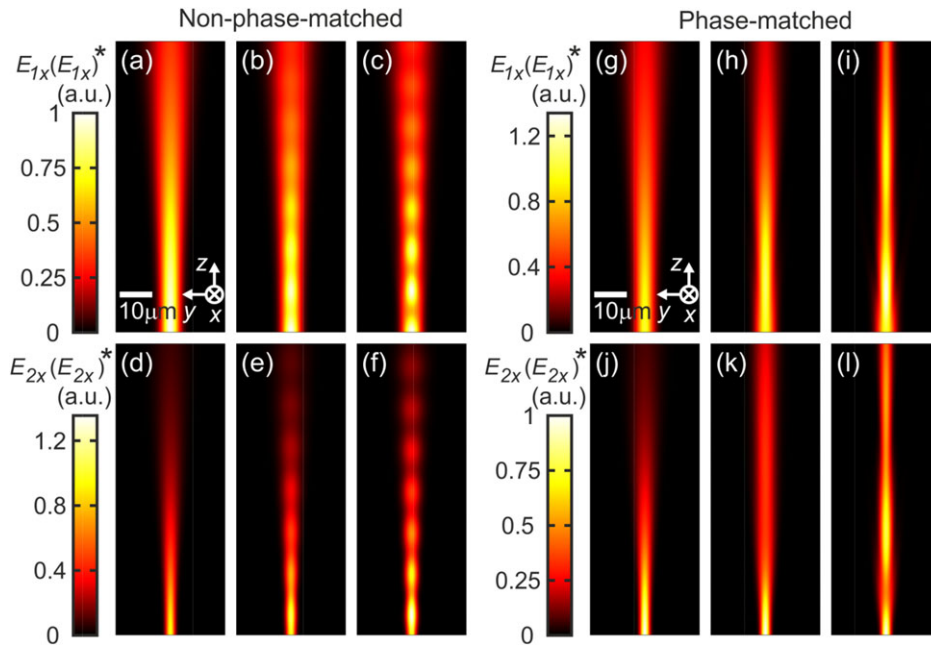


Figure 13. a)–f) Evolution of co-propagating fundamental and SH SPP beams in the non-phase-matched case $2k_1 - k_2 \gg 0$ (k_1 and k_2 are the wavenumbers of the fundamental and second-harmonic SPP beams, respectively). Linear propagation of (a) the fundamental and (d) the second-harmonic SPP beams in an effective 2D medium (mimicking Au/silica interface), the effective indices of the waves are $n_1^{eff} = 1.457 + 3.25 \times 10^{-4}i$ and $n_2^{eff} = 1.514 + 7.5 \times 10^{-4}i$ at 1500 and 750 nm wavelengths, respectively. Nonlinear propagation and self-focusing of (b, c) the fundamental and (e, f) the second-harmonic SPP beams for different light intensities corresponding to (b, e) $\chi^{(2)} E_1 = 0.02$ and (c, g) $\chi^{(2)} E_1 = 0.05$ nonlinearities. The initial amplitudes of both beams are equal ($E_1 = E_2$) and the beam half-widths are $w_{1,2} = 2.5\lambda_{1,2}$. g)–i) Corresponding fieldmaps for the phase-matched case with $\text{Re}(n_1^{eff}) = \text{Re}(n_2^{eff}) = 1.583$. Reproduced with permission.^[177] Copyright 2013, Institute of Physics.

frequencies. At the same time, the energy exchange between the beams can be seen: the maximum intensity of one beam corresponds to the minimum intensity of the other (Figure 13c and f). Furthermore, the effect of narrowing of the SPP beams, driven by the nonlinearity, can be seen in the decrease in the average beam width at both the fundamental frequency and the second-harmonic frequency. The largest modulation of the intensity profiles is in the centres of the beams, where intensities are the highest and the nonlinear coupling is the strongest.

The efficiency of this soliton formation process can be increased if the phase matching between the fundamental and second-harmonic SPPs is achieved. This can be introduced using as the SPP-supporting interface a dielectric medium with anomalous dispersion to compensate for the SPP dispersion: $\text{Re}(n_1^{eff}) = \text{Re}(n_2^{eff})$.^[1] The evolution of the SPP beams in both linear and nonlinear regimes in this case shows the evident transformation of the SPP modes into highly localised nondiffracting solitons, allowing to achieve SPP beams with a narrower spatial profile than in the absence of the phase matching. SPP self-focusing effect occurring near the excitation boundary was also observed (Figure 13i and l).

9. Conclusion

Various nanoplasmonic platforms based on planar and structured plasmonic-dielectric interfaces, plasmonic nanoparticles and their composites, as well as plasmonic metamaterials, facili-

tate enhancement and engineering of many nonlinear phenomena. Both spectrum and value of effective nonlinear susceptibilities can be manipulated in plasmonic environment. Nonlinear response can be introduced either by adjacent nonlinear optical materials in hybrid plasmonic structures or solely aided by inherent nonlinearities in plasmonic nanostructures themselves. In all cases, plasmonic structures provide strong field enhancement near the interfaces as well as flexible control over modal dispersions and strong sensitivity to the refractive index changes. All this enables plasmonic nanostructures to achieve both coherent and Kerr-type nonlinear responses on deep subwavelength scales, where majority of conventional dielectric components fail due to natural limitations, set by the diffraction limit and low values of nonlinearities requiring either long propagation range or very high light intensities. Flexible near-field manipulation in the vicinity of the nanostructures allows making use of spatially varying vectorial electromagnetic fields, and, thus, provides an opportunity to access all components of the nonlinear susceptibility tensor.

Another very important advantage of materials with free electrons in the field of nonlinear optics is their inherent and ultrafast nonlinear response due to the complex dynamics of electrons in strong electromagnetic fields. The most widely used models for describing this nontrivial electron dynamics in nanostructures are the hydrodynamic model, describing a free electron plasma with collective interactions between electrons, and the two-temperature model, taking into account non-equilibrium statistics of the carriers under optical excitation. Both models and

the respective nonlinear properties can be affected by the nanostructured geometry, resulting for truly nanoscale objects in the importance of nonlocal electromagnetic effects, which become significant at the length scale achievable with modern nanofabrication techniques. These nonlocal effects open a new route for engineering the nonlinear response.

In this review, we gave a brief general overview of the field of nonlinear plasmonics in a full hydrodynamic description. After discussing the origins of various nonlinear phenomena, plasmonic approaches for tailoring and enhancing nonlinearity were outlined, each time giving an illustration of the related vivid physical phenomena. This included coherent nonlinear effects, such as harmonic generation at the nanoscale and nonlinear coupling of plasmonic resonances (an analogue of phase-matching at the macroscale). A hydrodynamic time-domain numerical model was reviewed for coherent interactions of free-carrier plasma in a nanostructure of an arbitrary shape with an optical pulse of an arbitrary temporal profile, without any approximations. The approach allows to address the phenomena of multiple and resonantly-enhanced harmonic generation as well as reveals the interplay between the nonlinear effects and a topology of the nanostructure. Ultrafast Kerr-type nonlinearity due to the saturation of interband transitions and heating of a free-electron gas in the conduction band was overviewed with a particular example of engineering magnitude, spectrum and sign of the nonlinearity using a plasmonic nanorod metamaterial. At a designed wavelength, the metamaterial can provide either induced absorption or transparency and focusing or defocusing nonlinearity, depending on its geometrical parameters, opening up opportunities for custom-engineered nonlinear materials for switching and modulation of light with light. Nonlinear surface waves on the interfaces between linear and nonlinear media, including plasmon solitons and cascaded SPP solitons, were also briefly overviewed.

The use of plasmonic nanostructures in nonlinear optics has allowed to move nonlinear optical processes in a realm of integrated photonics as well as to demonstrate low-light intensity nonlinear effects for free-standing optical applications. Switching, controlling, routing and manipulating of light with light is a difficult but rewarding problem with the applications ranging from on-chip optical data processing and routing to nonlinear optical components for optical communication networks and laser applications. Plasmonics has helped to demonstrate many nonlinear optical effects on the subwavelength scales as well as in macroscopic implementations with much reduced required powers of light. Until recently, nonlinear plasmonic effects have mainly been demonstrated with conventional plasmonic materials, such as Au, Ag and Al. Unconventional phase changing plasmonic materials, such as Ga₂^[147,178,179] as well as ferromagnetic materials (Ni, Co) with a plasmonic response in visible and ultraviolet spectral regions were also considered.^[180–184] The development of a new type of plasmonic semiconductors based on nitrides and oxides, such as TiN, ITO, doped ZnO, as well as two-dimensional materials using plasmonic properties of graphene and transition metal dichalcogenides, including topological insulators and “Dirac-cone” materials, and plasmonic quantum dots has already started to provide a new push in nonlinear plasmonics.^[185–194] The use of new features that become accessible with the new materials as well as possible to engineer via appropriate nanostructuring in composite metamaterial arrange-

ments, e.g., epsilon-near-zero behaviour in technologically relevant spectral ranges, additionally enhances practical applications of nonlinear plasmonic components. Modern fabrication technologies have permitted the achievement of fine nanoscale control over the plasmonic geometries which allowed flexible tuning of their resonances to succeed in the design of high effective nonlinearities at the desired wavelengths and with short response times. We believe that the future of nonlinear optics in its various facets of free-space, integrated or quantum nanophotonic technologies will be shaped by nonlinear plasmonics.

Acknowledgements

This work has been supported, in part, by EPSRC (UK) and the ERC iPLASMM project (321268). P.G. acknowledges the support by the TAU Rector Grant and German-Israeli Foundation (GIF, grant number 2399). A.Z. acknowledges support from the Royal Society and the Wolfson Foundation.

Conflict of Interest

The authors have declared no conflict of interest.

Keywords

free-electron nonlinearity, harmonic generation, Kerr effect, nonlinear optics, plasmonics

Received: April 2, 2017

Revised: November 13, 2017

Published online: December 13, 2017

- [1] R. W. Boyd, *Nonlinear Optics*, 3rd ed., Academic Press, **2008**.
- [2] Y. R. Shen, *The Principles of Nonlinear Optics*, Wiley, **1984**.
- [3] W. L. Barnes, A. Dereux, T. W. Ebbesen, *Nature* **2003**, 424, 824.
- [4] A. V. Zayats, I. I. Smolyaninov, A. A. Maradudin, *Phys. Rep.* **2005**, 408, 131.
- [5] *Plasmonic Nanoguides and Circuits*, (Eds: S. I. Bozhevolnyi), Pan Stanford Publishing Pte. Ltd., **2009**.
- [6] *Active Plasmonics and Tuneable Plasmonic Metamaterials*, 1st ed., (Eds: A. V. Zayats, S. Maier), Wiley, **2013**.
- [7] *Optical Metamaterials: Fundamentals and Applications*, (Eds: W. Cai, V. Shalaev), Springer, **2009**.
- [8] *Modern Plasmonics*, (Eds: A. A. Maradudin, J. R. Sambles, W. L. Barnes), Elsevier, **2014**.
- [9] J. A. Schuller, E. S. Barnard, W. S. Cai, Y. C. Jun, J. S. White, M. L. Brongersma, *Nat. Mater.* **2010**, 9, 193.
- [10] M. Kauranen, A. V. Zayats, *Nat. Photonics* **2012**, 6, 737.
- [11] A. D. Boardman, A. V. Zayats, in *Modern Plasmonics*, (Eds: A. A. Maradudin, J. R. Sambles, W. L. Barnes), Elsevier, **2014**, p. 329.
- [12] A. D. Boardman, in *Electromagnetic Surface Modes*, (Eds: A. D. Boardman), Wiley, **1982**, p. 1.
- [13] F. Forstmann, R. R. Gerhardts, *Metal Optics Near the Plasma Frequency*, Springer-Verlag, **1986**.
- [14] J. E. Sipe, V. C. Y. So, M. Fukui, G. I. Stegeman, *Phys. Rev. B* **1980**, 21, 4389.
- [15] C. David, F. J. García de Abajo, *J. Phys. Chem. C* **2011**, 115, 19470.
- [16] R. Becker, F. Sauter, *Theorie der Elektrizität*, Vol. 3, Teubner, **1969**.
- [17] A. Eguiluz, J. J. Quinn, *Phys. Rev. B* **1976**, 14, 1347.

- [18] C. Ciraci, *Phys. Rev. B* **2017**, *95*, 245434.
- [19] R. H. Ritchie, *Phys. Rev.* **1957**, *106*, 874.
- [20] W. Yan, *Phys. Rev. B* **2015**, *91*, 115416.
- [21] A. Moradi, *Plasmonics* **2015**, *10*, 1225.
- [22] M. Scalora, M. A. Vincenti, D. de Ceglia, V. Roppo, M. Centini, N. Akozbek, M. J. Bloemer, *Phys. Rev. A* **2010**, *82*, 043828.
- [23] L. Stella, P. Zhang, F. J. García-Vidal, A. Rubio, P. García-González, *J. Phys. Chem. C* **2013**, *117*, 8941.
- [24] T. V. Teperik, P. Nordlander, J. Aizpurua, A. G. Borisov, *Opt. Express* **2013**, *21*, 27306.
- [25] R. Sundararaman, P. Narang, A. S. Jermyn, W. A. Goddard, 3rd., H. A. Atwater, *Nat. Commun.* **2014**, *5*, 5788.
- [26] H. Raether, *Surface Plasmons on Smooth and Rough Surfaces and Gratings*, Springer, **1988**.
- [27] A. V. Krasavin, A. V. Zayats, *Adv. Opt. Mater.* **2015**, *3*, 1662.
- [28] R. H. Ritchie, R. E. Wilems, *Phys. Rev.* **1969**, *178*, 372.
- [29] G. Barton, *Rep. Prog. Phys.* **1979**, *42*, 963.
- [30] J. M. Pitarke, V. M. Silkin, E. V. Chulkov, P. M. Echenique, *Rep. Prog. Phys.* **2007**, *70*, 1.
- [31] A. D. Boardman, B. V. Paranjape, Y. O. Nakamura, *Phys. Status Solidi B* **1976**, *75*, 347.
- [32] F. Forstmann, R. R. Gerhardts, in *Advances in Solid State Physics*, vol. 22, (Ed: P. Grosse Aachen), Vieweg, **1982**, p. 291.
- [33] S. Raza, S. I. Bozhevolnyi, M. Wubs, N. Asger Mortensen, *J. Phys. Condens. Matter* **2015**, *27*, 183204.
- [34] C. Ciraci, J. B. Pendry, D. R. Smith, *Chem. Phys. Chem.* **2013**, *14*, 1109.
- [35] S. Raza, N. Stenger, S. Kadkhodazadeh, S. V. Fischer, N. Kostesha, A.-P. Jauho, A. Burrows, M. Wubs, N. A. Mortensen, *Nanophotonics* **2013**, *2*, 131.
- [36] A. D. Boardman, B. V. Paranjape, *J. Phys. F* **1977**, *7*, 1935.
- [37] K. R. Hiremath, L. Zschiedrich, F. Schmidt, *J. Comput. Phys.* **2012**, *231*, 5890.
- [38] N. A. Mortensen, S. Raza, M. Wubs, T. Sondergaard, S. I. Bozhevolnyi, *Nat. Commun.* **2014**, *5*, 3809.
- [39] G. Toscano, J. Straubel, A. Kwiatkowski, C. Rockstuhl, F. Evers, H. Xu, N. A. Mortensen, M. Wubs, *Nat. Commun.* **2015**, *6*, 7132.
- [40] X. Li, H. Fang, X. Weng, L. Zhang, X. Dou, A. Yang, X. Yuan, *Opt. Express* **2015**, *23*, 29738.
- [41] C. Ciraci, F. Della Sala, *Phys. Rev. B* **2016**, *93*, 205405.
- [42] C. Tserkezis, N. Stefanou, M. Wubs, N. A. Mortensen, *Nanoscale* **2016**, *8*, 17532.
- [43] C. Ciraci, R. T. Hill, J. J. Mock, Y. Urzhumov, A. I. Fernandez-Dominguez, S. A. Maier, J. B. Pendry, A. Chilkoti, D. R. Smith, *Science* **2012**, *337*, 1072.
- [44] S. Raza, M. Wubs, S. I. Bozhevolnyi, N. A. Mortensen, *Opt. Lett.* **2015**, *40*, 839.
- [45] Q. S. Huang, F. L. Bao, S. L. He, *Opt. Express* **2013**, *21*, 1430.
- [46] G. Toscano, S. Raza, A. P. Jauho, N. A. Mortensen, M. Wubs, *Opt. Express* **2012**, *20*, 4176.
- [47] G. Toscano, S. Raza, S. Xiao, M. Wubs, A. P. Jauho, S. I. Bozhevolnyi, N. A. Mortensen, *Opt. Lett.* **2012**, *37*, 2538.
- [48] C. Ciraci, E. Poutrina, M. Scalora, D. R. Smith, *Phys. Rev. B* **2012**, *86*, 115451.
- [49] N. Bloembergen, R. K. Chang, S. S. Jha, C. H. Lee, *Phys. Rev.* **1968**, *174*, 813.
- [50] P. Ginzburg, A. Hayat, N. Berkovitch, M. Orenstein, *Opt. Lett.* **2010**, *35*, 1551.
- [51] A. V. Zayats, I. I. Smolyaninov, C. C. Davis, *Opt. Commun.* **1999**, *169*, 93.
- [52] F. Keilmann, R. Hillenbrand, *Philos. Trans. R. Soc. London Ser. A* **2004**, *362*, 787.
- [53] P. Ginzburg, A. Krasavin, Y. Sonnefraud, A. Murphy, R. J. Pollard, S. A. Maier, A. V. Zayats, *Phys. Rev. B* **2012**, *86*, 085422.
- [54] J. N. Anker, W. P. Hall, O. Lyandres, N. C. Shah, J. Zhao, R. P. Van Duyne, *Nat. Mater.* **2008**, *7*, 442.
- [55] A. V. Kabashin, P. Evans, S. Pastkovsky, W. Hendren, G. A. Wurtz, R. Atkinson, R. Pollard, V. A. Podolskiy, A. V. Zayats, *Nat. Mater.* **2009**, *8*, 867.
- [56] N. Vasilantonakis, G. A. Wurtz, V. A. Podolskiy, A. V. Zayats, *Opt. Express* **2015**, *23*, 14329.
- [57] R. W. Boyd, Z. Shi, I. De Leon, *Opt. Commun.* **2014**, *326*, 74.
- [58] O. Lysenko, M. Bache, N. Olivier, A. V. Zayats, A. Lavrinenko, *ACS Photonics* **2016**, *3*, 2324.
- [59] J. Dryzek, A. Czaplá, *Phys. Rev. Lett.* **1987**, *58*, 721.
- [60] A. V. Zayats, O. Keller, K. Pedersen, A. Liu, F. A. Pudonin, *IEEE J. Quantum Electron.* **1995**, *31*, 2044.
- [61] M. Perner, P. Bost, U. Lemmer, G. vonPlessen, J. Feldmann, U. Becker, M. Mennig, M. Schmitt, H. Schmidt, *Phys. Rev. Lett.* **1997**, *78*, 2192.
- [62] N. N. Lepeshkin, A. Schweinsberg, G. Piredda, R. S. Bennink, R. W. Boyd, *Phys. Rev. Lett.* **2004**, *93*, 123902.
- [63] G. Piredda, D. D. Smith, B. Wendling, R. W. Boyd, *J. Opt. Soc. Am. B* **2008**, *25*, 945.
- [64] J. Rudnick, E. A. Stern, *Phys. Rev. B* **1971**, *4*, 4274.
- [65] D. Maystre, M. Neviere, R. Reinisch, *Appl. Phys. A* **1986**, *39*, 115.
- [66] A. Benedetti, M. Centini, C. Sibilia, M. Bertolotti, *J. Opt. Soc. Am. B* **2010**, *27*, 408.
- [67] C. Ciraci, E. Poutrina, M. Scalora, D. R. Smith, *Phys. Rev. B* **2012**, *85*, 201403(R).
- [68] F. X. Wang, F. J. Rodríguez, W. M. Albers, R. Ahorinta, J. E. Sipe, M. Kauranen, *Phys. Rev. B* **2009**, *80*, 233402.
- [69] C. Forestiere, A. Capretti, G. Miano, *J. Opt. Soc. Am. B* **2013**, *30*, 2355.
- [70] G. Bachelier, J. Butet, I. Russier-Antoine, C. Jonin, E. Benichou, P. F. Brevet, *Phys. Rev. B* **2010**, *82*, 235403.
- [71] N. W. Ashcroft, N. Mermin, *Solid State Physics*, Brooks/Cole, **1976**.
- [72] D. R. Nicholson, *Introduction to Plasma Theory*, Wiley, **1983**.
- [73] L. Jiang, H.-L. Tsai, *J. Heat Transfer* **2005**, *127*, 1167.
- [74] A. D. Neira, N. Olivier, M. E. Nasir, W. Dickson, G. A. Wurtz, A. V. Zayats, *Nat. Commun.* **2015**, *6*, 7757.
- [75] J. Bigot, J. Merle, O. Cregut, A. Daunois, *Phys. Rev. Lett.* **1995**, *75*, 4702.
- [76] D. Pines, *Elementary Excitations in Solids: Lectures on Protons, Electrons, and Plasmons*, Perseus Books, **1999**.
- [77] S. Peruch, A. Neira, G. A. Wurtz, B. Wells, V. A. Podolskiy, A. V. Zayats, *Adv. Opt. Mater.* **2017**, *5*, 1700299.
- [78] J. Butet, P. F. Brevet, O. J. F. Martin, *ACS Nano* **2015**, *9*, 10545.
- [79] X. M. Hua, J. I. Gersten, *Phys. Rev. B* **1986**, *33*, 3756.
- [80] D. Ostling, P. Stampfli, K. H. Bennemann, *Z. Phys. D* **1993**, *28*, 169.
- [81] P. Guyot-Sionnest, Y. R. Shen, *Phys. Rev. B* **1988**, *38*, 7985.
- [82] A. Benedetti, M. Centini, M. Bertolotti, C. Sibilia, *Opt. Express* **2011**, *19*, 26752.
- [83] A. Capretti, C. Forestiere, L. Dal Negro, G. Miano, *Plasmonics* **2013**, *9*, 151.
- [84] J. I. Dadap, J. Shan, K. B. Eisenthal, T. F. Heinz, *Phys. Rev. Lett.* **1999**, *83*, 4045.
- [85] J. I. Dadap, J. Shan, T. F. Heinz, *J. Opt. Soc. Am. B* **2004**, *21*, 1328.
- [86] Y. Pavlyukh, W. Hübner, *Phys. Rev. B* **2004**, *70*, 245434.
- [87] J. Nappa, G. Revillod, I. Russier-Antoine, E. Benichou, C. Jonin, P. F. Brevet, *Phys. Rev. B* **2005**, *71*, 165407.
- [88] I. Russier-Antoine, E. Benichou, G. Bachelier, C. Jonin, P. F. Brevet, *J. Phys. Chem. C* **2007**, *111*, 9044.
- [89] G. Bachelier, I. Russier-Antoine, E. Benichou, C. Jonin, P. F. Brevet, *J. Opt. Soc. Am. B* **2008**, *25*, 955.
- [90] Smolyaninov, II, A. V. Zayats, C. C. Davis, *Phys. Rev. B* **1997**, *56*, 9290.

- [91] A. V. Zayats, T. Kalkbrenner, V. Sandoghdar, J. Mlynek, *Phys. Rev. B* **2000**, *61*, 4545.
- [92] R. Kolkowski, J. Szeszko, B. Dwir, E. Kapon, J. Zyss, *Laser Photonics Rev.* **2016**, *10*, 287.
- [93] B. L. Wang, R. Wang, R. J. Liu, X. H. Lu, J. Zhao, Z. Y. Li, *Sci. Rep.* **2013**, *3*, 2358.
- [94] K. O'Brien, H. Suchowski, J. Rho, A. Salandrino, B. Kante, X. Yin, X. Zhang, *Nat. Mater.* **2015**, *14*, 379.
- [95] M. Celebrano, X. Wu, M. Baselli, S. Grossmann, P. Biagioni, A. Locatelli, C. De Angelis, G. Cerullo, R. Osellame, B. Hecht, L. Duo, F. Ciccacci, M. Finazzi, *Nat. Nanotechnol.* **2015**, *10*, 412.
- [96] M. L. Ren, S. Y. Liu, B. L. Wang, B. Q. Chen, J. Li, Z. Y. Li, *Opt. Express* **2014**, *22*, 28653.
- [97] J. Butet, O. J. F. Martin, *J. Opt. Soc. Am. B* **2016**, *33*, A8.
- [98] B. K. Canfield, H. Husu, J. Laukkanen, B. F. Bai, M. Kuittinen, J. Turunen, M. Kauranen, *Nano Lett.* **2007**, *7*, 1251.
- [99] M. I. Shalaev, Z. A. Kudyshev, N. M. Litchinitser, *Opt. Lett.* **2013**, *38*, 4288.
- [100] M. W. Klein, C. Enkrich, M. Wegener, S. Linden, *Science* **2006**, *313*, 502.
- [101] N. Feth, S. Linden, M. W. Klein, M. Decker, F. B. P. Niesler, Y. Zeng, W. Hoyer, J. Liu, S. W. Koch, J. V. Moloney, M. Wegener, *Opt. Lett.* **2008**, *33*, 1975.
- [102] K. A. O'Donnell, R. Torre, C. S. West, *Phys. Rev. B* **1997**, *55*, 7985.
- [103] M. I. Stockman, D. J. Bergman, C. Anceau, S. Brasselet, J. Zyss, *Phys. Rev. Lett.* **2004**, *92*, 057402.
- [104] T. Stefaniuk, N. Olivier, A. Belardini, C. P. T. McPolin, C. Sibilia, A. A. Wronkowska, A. Wronkowski, T. Szoplik, A. V. Zayats, *Adv. Opt. Mater.*, **2017**, *5*, 1700753.
- [105] J. Butet, K. Thyagarajan, O. J. Martin, *Nano Lett.* **2013**, *13*, 1787.
- [106] G. Bautista, M. J. Huttunen, J. Makitalo, J. M. Kontio, J. Simonen, M. Kauranen, *Nano Lett.* **2012**, *12*, 3207.
- [107] J. P. Dewitz, W. Hubner, K. H. Bennemann, *Z. Phys. D* **1996**, *37*, 75.
- [108] D. Carroll, X. H. Zheng, *Eur. Phys. J. D* **1999**, *5*, 135.
- [109] Y. Yu, S.-S. Fan, H.-W. Dai, Z.-W. Ma, X. Wang, J.-B. Han, L. Li, *Appl. Phys. Lett.* **2014**, *105*, 061903.
- [110] B. Metzger, M. Hentschel, M. Nesterov, T. Schumacher, M. Lippitz, H. Giessen, *Appl. Phys. B* **2016**, *122*, 77.
- [111] J. B. Lassiter, X. Chen, X. Liu, C. Ciraci, T. B. Hoang, S. Larouche, S.-H. Oh, M. H. Mikkelsen, D. R. Smith, *ACS Photonics* **2014**, *1*, 1212.
- [112] K. Li, X. Li, D. Yuan Lei, S. Wu, Y. Zhan, *Appl. Phys. Lett.* **2014**, *104*, 261105.
- [113] M. S. Nezami, R. Gordon, *Opt. Express* **2015**, *23*, 32006.
- [114] G. Hajisalem, D. K. Hore, R. Gordon, *Opt. Mater. Express* **2015**, *5*, 2217.
- [115] T. Wu, P. P. Shum, Y. Sun, X. Shao, T. Huang, *Opt. Express* **2015**, *23*, 253.
- [116] A. E. Minovich, A. E. Miroshnichenko, A. Y. Bykov, T. V. Murzina, D. N. Neshev, Y. S. Kivshar, *Laser Photonics Rev.* **2015**, *9*, 195.
- [117] M. Ren, E. Plum, J. Xu, N. I. Zheludev, *Nat. Commun.* **2012**, *3*, 833.
- [118] S. Linden, F. B. Niesler, J. Forstner, Y. Grynko, T. Meier, M. Wegener, *Phys. Rev. Lett.* **2012**, *109*, 015502.
- [119] J. Alberti, H. Linnenbank, S. Linden, Y. Grynko, J. Forstner, *Appl. Phys. B* **2016**, *122*, 5.
- [120] G. Marino, P. Segovia, A. V. Krasavin, P. Ginzburg, N. Olivier, G. A. Wurtz, A. V. Zayats, *Laser Photonics Rev.* (in press).
- [121] P. Segovia, G. Marino, A. V. Krasavin, N. Olivier, G. A. Wurtz, P. A. Belov, P. Ginzburg, A. V. Zayats, *Opt. Express* **2015**, *23*, 30730.
- [122] P. Ginzburg, A. V. Krasavin, G. A. Wurtz, A. V. Zayats, *ACS Photonics* **2015**, *2*, 8.
- [123] A. V. Krasavin, P. Ginzburg, G. A. Wurtz, A. V. Zayats, *Nat. Commun.* **2016**, *7*, 11497.
- [124] J. I. Dadap, *Phys. Rev. B* **2008**, *78*, 205322.
- [125] P. Ginzburg, A. V. Zayats, *ACS Nano* **2013**, *7*, 4334.
- [126] R. B. Davidson Ii, J. I. Ziegler, G. Vargas, S. M. Avanesyan, Y. Gong, W. Hess, R. F. Haglund Jr., *Nanophotonics* **2015**, *4*, 108.
- [127] D. N. Nikogosyan, *Nonlinear Optical Crystals: A Complete Survey*, Springer Science Business Media, Inc., **2005**.
- [128] Y. Zhang, N. K. Grady, C. Ayala-Orozco, N. J. Halas, *Nano Lett.* **2011**, *11*, 5519.
- [129] C. K. Sun, F. Vallée, L. Acioli, E. P. Ippen, J. G. Fujimoto, *Phys. Rev. B* **1993**, *48*, 12365.
- [130] N. Del Fatti, R. Bouffanais, F. Vallee, C. Flytzanis, *Phys. Rev. Lett.* **1998**, *81*, 922.
- [131] M. I. Stockman, *Opt. Express* **2011**, *19*, 22029.
- [132] S. Link, M. A. El-Sayed, *J. Phys. Chem. B* **1999**, *103*, 8410.
- [133] M. Pelton, J. Aizpurua, G. Bryant, *Laser Photonics Rev.* **2008**, *2*, 136.
- [134] H. Baida, D. Mongin, D. Christofilos, G. Bachelier, A. Crut, P. Maioli, N. Del Fatti, F. Vallee, *Phys. Rev. Lett.* **2011**, *107*, 057402.
- [135] M. Halonen, A. A. Lipovskii, Y. P. Svirko, *Opt. Express* **2007**, *15*, 6840.
- [136] G. Ma, W. Sun, S. H. Tang, H. Zhang, Z. Shen, S. Qian, *Opt. Lett.* **2002**, *27*, 1043.
- [137] M. Abb, P. Albella, J. Aizpurua, O. L. Muskens, *Nano Lett.* **2011**, *11*, 2457.
- [138] Y. Lin, X. Zhang, X. Fang, S. Liang, *Nanoscale* **2016**, *8*, 1421.
- [139] G. Della Valle, D. Polli, P. Biagioni, C. Martella, M. C. Giordano, M. Finazzi, S. Longhi, L. Duò, G. Cerullo, F. Buatier de Mongeot, *Phys. Rev. B* **2015**, *91*, 235440.
- [140] M. Pohl, V. I. Belotelov, I. A. Akimov, S. Kasture, A. S. Vengurlekar, A. V. Gopal, A. K. Zvezdin, D. R. Yakovlev, M. Bayer, *Phys. Rev. B* **2012**, *85*, 081401(R).
- [141] X. Wang, R. Morea, J. Gonzalo, B. Palpant, *Nano Lett.* **2015**, *15*, 2633.
- [142] N. Rotenberg, M. Betz, H. M. van Driel, *Phys. Rev. Lett.* **2010**, *105*, 017402.
- [143] N. Rotenberg, M. Betz, H. M. Van Driel, *Opt. Lett.* **2008**, *33*, 2137.
- [144] C. P. T. McPolin, N. Olivier, J.-S. Bouillard, D. O'Connor, A. V. Krasavin, W. Dickson, G. A. Wurtz, A. V. Zayats, *Light Sci. Appl.* **2017**, *6*, e16237.
- [145] L. H. Nicholls, F. J. Rodriguez-Fortuno, M. E. Nasir, R. M. Cordova-Castro, N. Olivier, G. A. Wurtz, A. V. Zayats, *Nat. Photonics* **2017**, *11*, 628.
- [146] N. E. Khokhlov, D. O. Ignatyeva, V. I. Belotelov, *Opt. Express* **2014**, *22*, 28019.
- [147] A. V. Krasavin, N. I. Zheludev, *Appl. Phys. Lett.* **2004**, *84*, 1416.
- [148] D. Pacifici, H. J. Lezec, H. A. Atwater, *Nat. Photonics* **2007**, *1*, 402.
- [149] R. A. Pala, K. T. Shimizu, N. A. Melosh, M. L. Brongersma, *Nano Lett.* **2008**, *8*, 1506.
- [150] A. V. Krasavin, A. V. Zayats, *Phys. Rev. B* **2008**, *78*, 045425.
- [151] A. V. Krasavin, A. V. Zayats, *Opt. Commun.* **2010**, *283*, 1581.
- [152] A. V. Krasavin, S. Randhawa, J. S. Bouillard, J. Renger, R. Quidant, A. V. Zayats, *Opt. Express* **2011**, *19*, 25222.
- [153] S. Randhawa, A. V. Krasavin, T. Holmgaard, J. Renger, S. I. Bozhevolnyi, A. V. Zayats, R. Quidant, *Appl. Phys. Lett.* **2011**, *98*, 161102.
- [154] G. Sartorello, N. Olivier, J. J. Zhang, W. S. Yue, D. J. Gosztola, G. P. Wiederrecht, G. Wurtz, A. V. Zayats, *ACS Photonics* **2016**, *3*, 1517.
- [155] C. M. Soukoulis, M. Wegener, *Nat. Photonics* **2011**, *5*, 523.
- [156] M. Ren, B. Jia, J. Y. Ou, E. Plum, J. Zhang, K. F. MacDonald, A. E. Nikolaenko, J. Xu, M. Gu, N. I. Zheludev, *Adv. Mater.* **2011**, *23*, 5540.
- [157] K. T. Tsai, G. A. Wurtz, J. Y. Chu, T. Y. Cheng, H. H. Wang, A. V. Krasavin, J. H. He, B. M. Wells, V. A. Podolskiy, J. K. Wang, Y. L. Wang, A. V. Zayats, *Nano Lett.* **2014**, *14*, 4971.
- [158] P. Ginzburg, D. J. Roth, M. E. Nasir, P. Segovia, A. V. Krasavin, J. Levitt, L. M. Hirvonen, B. Wells, K. Suhling, D. Richards, V. A. Podolskiy, A. V. Zayats, *Light Sci. Appl.* **2017**, *6*, e16273.
- [159] D. J. Roth, A. V. Krasavin, A. Wade, W. Dickson, A. Murphy, S. Kena-Cohen, R. Pollard, G. A. Wurtz, D. Richards, S. A. Maier, A. V. Zayats, *ACS Photonics* **2017**, *4*, 2513.

- [160] R. J. Pollard, A. Murphy, W. R. Hendren, P. R. Evans, R. Atkinson, G. A. Wurtz, A. V. Zayats, V. A. Podolskiy, *Phys. Rev. Lett.* **2009**, *102*, 127405.
- [161] B. M. Wells, A. V. Zayats, V. A. Podolskiy, *Phys. Rev. B* **2014**, *89*, 035111.
- [162] V. A. Podolskiy, P. Ginzburg, B. Wells, A. V. Zayats, *Faraday Discuss.* **2015**, *178*, 61.
- [163] G. A. Wurtz, R. Pollard, W. Hendren, G. P. Wiederrecht, D. J. Gosztola, V. A. Podolskiy, A. V. Zayats, *Nat. Nanotechnol.* **2011**, *6*, 107.
- [164] A. D. Neira, G. A. Wurtz, P. Ginzburg, A. V. Zayats, *Opt. Express* **2014**, *22*, 10987.
- [165] A. V. Krasavin, A. V. Zayats, *Proc. IEEE* **2016**, *104*, 2338.
- [166] N. Vasilantonakis, M. E. Nasir, W. Dickson, G. A. Wurtz, A. V. Zayats, *Laser Photonics Rev.* **2015**, *9*, 345.
- [167] M. Z. Alam, I. De Leon, R. W. Boyd, *Science* **2016**, *352*, 795.
- [168] Q. B. Guo, Y. H. Yao, Z. C. Luo, Z. P. Qin, G. Q. Xie, M. Liu, J. Kang, S. Zhang, G. Bi, X. F. Liu, J. R. Qiu, *ACS Nano* **2016**, *10*, 9463.
- [169] A. Baron, S. Larouche, D. J. Gauthier, D. R. Smith, *J. Opt. Soc. Am. B* **2014**, *32*, 9.
- [170] A. Baron, T. B. Hoang, C. Fang, M. H. Mikkelsen, D. R. Smith, *Phys. Rev. B* **2015**, *91*, 195412.
- [171] I. De Leon, Z. Shi, A. C. Liapis, R. W. Boyd, *Opt. Lett.* **2014**, *39*, 2274.
- [172] *Progress in Optics*, Vol. 27, (Eds: E. Wolf), Elsevier Science Publishers, **1989**.
- [173] Y. N. Karamzin, A. P. Sukhorukov, *Sov. Phys.—JETP* **1976**, *41*, 414.
- [174] W. E. Torruellas, Z. Wang, D. J. Hagan, E. W. VanStryland, G. I. Stegeman, L. Torner, C. R. Menyuk, *Phys. Rev. Lett.* **1995**, *74*, 5036.
- [175] R. Schiek, Y. Baek, G. I. Stegeman, *Phys. Rev. E* **1996**, *53*, 1138.
- [176] L. Torner, A. Barthelemy, *IEEE J. Quantum Electron.* **2003**, *39*, 22.
- [177] P. Ginzburg, A. V. Krasavin, A. V. Zayats, *New J. Phys.* **2013**, *15*, 013031.
- [178] A. V. Krasavin, K. F. MacDonald, A. S. Schwanecke, N. I. Zheludev, *Appl. Phys. Lett.* **2006**, *89*, 031118.
- [179] K. F. MacDonald, A. V. Krasavin, N. I. Zheludev, *Opt. Commun.* **2007**, *278*, 207.
- [180] V. L. Krutyanskiy, I. A. Kolmychek, E. A. Gan'shina, T. V. Murzina, P. Evans, R. Pollard, A. A. Stashkevich, G. A. Wurtz, A. V. Zayats, *Phys. Rev. B* **2013**, *87*, 035116.
- [181] V. K. Valev, A. V. Silhanek, W. Gillijns, Y. Jeyaram, H. Pad-dubrouskaya, A. Volodin, C. G. Biris, N. C. Panoiu, B. De Clercq, M. Ameloot, O. A. Aktsipetrov, V. V. Moshchalkov, T. Verbiest, *ACS Nano* **2011**, *5*, 91.
- [182] V. Bonanni, S. Bonetti, T. Pakizeh, Z. Pirzadeh, J. N. Chen, J. Nogues, P. Vavassori, R. Hillenbrand, J. Akerman, A. Dmitriev, *Nano Lett.* **2011**, *11*, 5333.
- [183] T. V. Murzina, T. V. Misuryaev, A. F. Kravets, J. Gudde, D. Schu-macher, G. Marowsky, A. A. Nikulin, O. A. Aktsipetrov, *Surf. Sci.* **2001**, *482*, 1101.
- [184] I. Rzdolski, D. Makarov, O. G. Schmidt, A. Kirilyuk, T. Rasing, V. V. Temnov, *ACS Photon.* **2016**, *3*, 179.
- [185] A. Boltasseva, H. A. Atwater, *Science* **2011**, *331*, 290.
- [186] H. Zhang, S. Virally, Q. L. Bao, L. K. Ping, S. Massar, N. Godbout, P. Kockaert, *Opt. Lett.* **2012**, *37*, 1856.
- [187] J. D. Cox, I. Silveiro, F. J. G. de Abajo, *ACS Nano* **2016**, *10*, 1995.
- [188] R. I. Woodward, R. T. Murray, C. F. Phelan, R. E. P. de Oliveira, T. H. Runcorn, E. J. R. Kelleher, S. Li, E. C. de Oliveira, G. J. M. Fechine, G. Eda, C. J. S. de Matos, *2D Mater.* **2017**, *4*, 011006.
- [189] U. Guler, A. Boltasseva, V. M. Shalaev, *Science* **2014**, *344*, 263.
- [190] G. V. Naik, V. M. Shalaev, A. Boltasseva, *Adv. Mater.* **2013**, *25*, 3264.
- [191] R. W. Yu, J. D. Cox, F. J. G. de Abajo, *Phys. Rev. Lett.* **2016**, *117*, 123904.
- [192] J. J. Dean, H. M. van Driel, *Appl. Phys. Lett.* **2009**, *95*, 261910.
- [193] S. A. Mikhailov, *Phys. Rev. B* **2011**, *84*, 045432.
- [194] J. L. Cheng, N. Vermeulen, J. E. Sipe, *New J. Phys.* **2014**, *16*, 053014.